Many-body order parameters for multipoles in solids

Byungmin Kang, Ken Shiozaki, and Gil Young Cho

Phys. Rev. B **100**, 245134 — Published 20 December 2019

DOI: 10.1103/PhysRevB.100.245134

Many-Body Order Parameters for Multipoles in Solids

Byungmin Kang,[1] Ken Shiozaki,[2] and Gil Young Cho[3,*]

[1] *School of Physics, Korea Institute for Advanced Study, Seoul 02455, Korea*
[2] *Yukawa Institute for Theoretical Physics, Kyoto University, Kyoto 606-8502, Japan*
[3] *Department of Physics, Pohang University of Science and Technology (POSTECH), Pohang 37673, Republic of Korea*

(Dated: November 11, 2019)

We propose many-body order parameters for bulk multipoles in crystalline systems, whenever the bulk multipole moments can be defined in terms of the nontrivial topology of the nested Wilson loop. The many-body order parameters are designed to measure multipolar charge distribution in a crystalline unit cell, and they match the localized corner charge originating from the multipoles when the symmetries quantizing the multipoles are protected. Our many-body order parameters provide complementary view to the nested Wilson loop approaches and even go beyond, as our many-body order parameters are readily applicable to interacting quantum many-body systems. Furthermore, even when the symmetries quantizing multipoles are lost so that the nested Wilson loop spectrum does not exactly reproduce the physical multipole moments, our many-body order parameters faithfully measure the physical multipole moments which is confirmed numerically during Thouless pumping processes. We provide analytic arguments and numerical demonstration of the order parameters for various higher-order insulators having bulk multipole moments. Finally, we discuss the applicability of our many-body order parameters in the cases where the Wannier gap is absent so that the bulk multiple moments cannot be defined in terms of the nested Wilson loop.

I. INTRODUCTION

Theory of macroscopic polarization in a crystal lies at the heart of the modern development of topological band insulators.[1] The theory provides a classic example of how the non-trivial topology of bulk ground states can determine the quintessential properties of the quantum phases such as symmetry-enforced boundary states.[2,3] Furthermore, it nicely illustrates how the associated topology can and cannot be diagnosed; the topology cannot be measured by a local operator, but only through a gauge-invariant number defined in a momentum space referred as the Zak phase,[4] or through a non-local many-body order parameter.[5] In particular, the discovery of the many-body order parameters, or equivalently "invariants", for various topological insulators drastically increased our understanding of topological states and expanded the range of the search for the topological states beyond free-fermion limits, e.g., strongly-correlated systems and bosonic models.[6–10]

Recently, a new class of topological states, namely higher-order topological insulators, has been discovered.[11–19] Interestingly, these higher-order states are constructed out of the electric multipoles, which materialize as topologically-protected modes at the corners and hinges of the physical boundary. To characterize such higher-order topology, the so-called "nested Wilson loop" approach[12] has been put forward and used to detect the quantized multipoles, by keeping track of all the relevant crystalline symmetries. However, a new class of higher-order topological insulator has been introduced under the name an anomalous topological insulator[19] whose non-trivial multipole moments cannot be diagnosed by a naive application of the nested Wilson loop approach. Moreover, the nested Wilson loop is genuinely a free-fermion quantity and thus cannot be a generic diagnosis for the higher-order topology in a general many-body condensed matter system. This opens a question how to measure multipole moments going beyond the nested Wilson loop picture.

Motivated from these, we propose a new set of many-body order parameters for the multipoles in crystalline systems, which are presented in Sec. II. In Sec. III, we explain our order parameters based on effective field-theoretic interpretation. In Sect. IV, we demonstrate that our many-body order parameters successfully measure the quantized bulk multipole moments for various higher-order topological insulators. In Sec. V, we discuss the applicability of our order parameters to the cases where the quantizing symmetries are lost. We have demonstrated numerically that using our many-body order parameter as the measure for quadrupole moment, the bulk-boundary correspondence holds for various models having non-quantized quadrupole moments. We conclude in Sec. VI, which are followed by Appendices where we discuss various aspects of our order parameters as well as the applicability of our order parameters in the cases where the Wannier gap is absence so that the bulk multipole moment cannot be defined in terms of the nested Wilson loop.

II. MANY-BODY ORDER PARAMETERS

A. Resta's Operator for Multipole Moments

We now introduce a set of many-body order parameters for multipole moments in solids. In stark contrast to the nested Wilson loop approaches, we utilize real-space charge distribution, which can be evaluated even for strongly-correlated systems. To this end, we extend Resta's general definition of polarization[5] to the multi-

poles:

$$P_x = \frac{1}{2\pi}\mathrm{Im}\left[\log\langle\hat{U}_1\rangle\right], \quad \hat{U}_1 = e^{2\pi i \sum_x \hat{p}_x}, \tag{1}$$

where $\hat{p}_x = \frac{x\hat{n}(x)}{L_x}$ is the polarization density (relative to $x = 0$) in the system of the length L_x with $\hat{n}(x)$ being the electron number operator at site x, and the sum is running over the whole system. Here the expectation value $\langle\hat{U}_1\rangle$ is over the many-body ground state subject to the periodic boundary condition, i.e., $x \sim x + L_x$. Compared to the Berry-phase expression[4] defined in momentum space, the above formula Eq. (1) provides a clearer picture of the macroscopic polarization P_x by relating it to the local microscopic polarization density $\hat{p}_x$.

Here, we propose an order parameter for quadrupole moment in a crystal as following:

$$Q_{xy} = \frac{1}{2\pi}\mathrm{Im}\left[\log\langle\hat{U}_2\rangle\right], \quad \hat{U}_2 = e^{2\pi i \sum_{\boldsymbol{r}} \hat{q}_{xy}(\boldsymbol{r})}. \tag{2}$$

Here $\hat{q}_{xy} = \frac{xy}{L_x L_y}\hat{n}(\boldsymbol{r})$ is the quadrupole moment density (relative to $x = y = 0$) per unit cell at the site $\boldsymbol{r}$. Similar to Eq. (1), L_x and L_y are the sizes of the system, and the sum is over $(x, y) \in (0, L_x] \times (0, L_y]$. Analogously, the macroscopic octupole moment can be measured as:

$$O_{xyz} = \frac{1}{2\pi}\mathrm{Im}\left[\log\langle\hat{U}_3\rangle\right], \quad \hat{U}_3 = e^{2\pi i \sum_{\boldsymbol{r}} \hat{o}_{xyz}(\boldsymbol{r})}. \tag{3}$$

Here $\hat{o}_{xyz} = \frac{xyz}{L_x L_y L_z}\hat{n}(\boldsymbol{r})$ is the octupole moment density per unit cell; the generalizations to higher-order poles follows immediately. As in the Resta's formula, we use a many-body ground state defined on the torus with periodic boundary conditions and each multipole moment density is summed over the whole space. Our real-space formula provides a complementary view to the momentum space approach, the nested Wilson loop indices.[12] In the remaining paper, we present supporting evidences that these many-body order parameters correctly measure the bulk multipole moments whenever the bulk multipole moments can be defined in terms of the nontrivial topology of the nested Wilson loop.[12] On the other hand, when the Wannier gap is absent so that the bulk multipole moments cannot be defined in terms of the nested Wilson loop, we find that our formula Eq. (2) does not show stable values against adiabatic deformations that preserve the bulk gap. (Please refer to Appendix E for more details on the behavior of $\hat{U}_2$ on various C_4-symmetric insulators.[20])

A few remarks are in order. First, the multipole moments defined as above are ambiguous up to "mod 1" because of the periodicity of complex phases; this ambiguity reproduces the observation made in the previous studies.[11,12] Second, we emphasize that the above expressions are truly many-body quantities because, when the exponentials are expanded, they require to measure $\sim \sum_{\boldsymbol{r}_1,\boldsymbol{r}_2,\cdots,\boldsymbol{r}_J}\langle\hat{n}(\boldsymbol{r}_1)\hat{n}(\boldsymbol{r}_2)\cdots\hat{n}(\boldsymbol{r}_J)\rangle$, and this does not reduce to the product of the few-particle observables. To evaluate Eq. (2) and Eq. (3), we need the full knowledge of the many-body ground state. On the other hand, the expressions are gauge-invariant, i.e., it is independent of the basis choice, and thus they measure physical quantities.

We can also show that the expressions Eq. (2) and Eq. (3) are invariant under the superposition of the trivial atomic insulator to the system. For example, let us take Eq. (2) and $L_x \cdot L_y$ being odd. Now, first consider a ground state $|GS_{\mathrm{triv}}\rangle = \otimes_x|\hat{n}_x = 1\rangle$ of an atomic trivial insulator, which has $\langle\hat{U}_2\rangle = 1$. When such a ground state is superposed with the topological state $|GS_{\mathrm{top}}\rangle$, i.e., $|GS_{\mathrm{new}}\rangle = |GS_{\mathrm{top}}\rangle \otimes |GS_{\mathrm{triv}}\rangle$, the quadrupole moment remains the same as before

$$\mathrm{Im}\log\langle GS_{\mathrm{top}}|\hat{U}_2|GS_{\mathrm{top}}\rangle = \mathrm{Im}\log\langle GS_{\mathrm{new}}|\hat{U}_2|GS_{\mathrm{new}}\rangle,$$

and hence showing the stability against addition of trivial bands (without turning on the coupling to the topological states).[21] This shows that our order parameters Eq. (2) and Eq. (3) measure certain topological properties of the insulators. To further identify them as the "order parameters" for the multipoles, we need a few more steps, which we present below.

B. Symmetry Considerations

We argue that Eq. (2) and Eq. (3) capture the symmetries of multipole moments properly. Let us concentrate on the quadrupole moment Eq. (2) for clarity. Below we choose our system to be on a torus $(x, y) \in (0, L_x] \times (0, L_y]$ and subject to the periodic boundary conditions $x + L_x \sim x$ and $y + L_y \sim y$. The effect of other coordinate parametrization is discussed in Appendix D 2 b.

First, note that under the mirrors $\{\mathcal{M}_x, \mathcal{M}_y\}$, our Eq. (2) transforms as $\hat{U}_2 \to \hat{U}_2^*$, where asterisk denotes the complex conjugation, and thus $Q_{xy} \to -Q_{xy}$. (We defer a more careful analysis of the symmetry actions including C_4 symmetry to Appendix A.)

Second, we can also intuitively understand why the polarization must vanish for the quadrupole moment to be well-defined. To this end, we perform $x \to x + L_x$ globally, which maps $\hat{U}_2 \to \hat{U}_2' = \hat{U}_2\hat{U}_{1;y}$ where $\hat{U}_{1;y} = \exp[2\pi i/L_y \sum_y y\hat{n}(\boldsymbol{r})] = \exp(2\pi i\hat{\mathcal{P}}_y)$. Although $\langle\hat{U}_2\rangle \neq \langle\hat{U}_2'\rangle$ in general (because the ground state is not generally an eigenstate of $\hat{U}_{1;y}$), we find

$$\langle\hat{U}_2'\rangle = \langle\hat{U}_2\rangle\langle\hat{U}_{1;y}\rangle + \mathcal{O}(\frac{1}{E_{\mathrm{gap}}}),$$

where E_{gap} is the excitation gap, which is inversely proportional to the correlation length.[6,22] In the ideal limit $E_{\mathrm{gap}} \to \infty$, we can see that the quadrupole moment, which is the imaginary part of $\langle\hat{U}_2\rangle$, is well-defined when the polarization vanishes. Similarly, the total polarization $\hat{\mathcal{P}}_x$ along x must vanish to have a well-defined

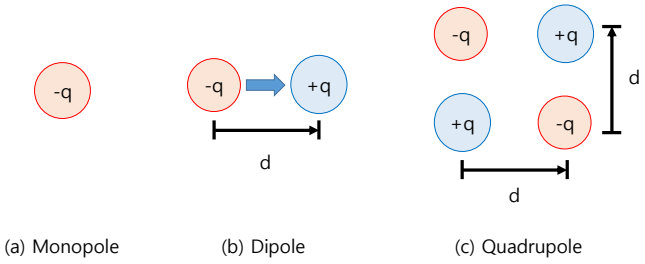

FIG. 1. Charge configuration in real space with multipole moments

quadrupole moment. By passing, we note that this invariance of $\langle \hat{U}_2 \rangle$ up to the perturbative correction is *weaker* than the original Resta's formula Eq. (1) where $x \to x + L_x$ is an exact symmetry. Though we have shown that the polarization at $E_{\rm gap} \to \infty$ must vanish to have a well-defined quadrupole moment, the polarization is invariant under the adiabatic change of the gap when the quantizing symmetries present and thus the same conclusion should apply to the finite-gap systems with quantizing symmetries.

III. EFFECTIVE FIELD THEORY OF THE MULTIPOLES

In this section, we derive the effective response from the semi-classical picture and then use it to reproduce the essential features[12] of the topological quadrupolar insulators. Furthermore, we also show the link between the ground state expectation value $\langle \hat{U}_a \rangle$ and the partition function. Motivated from the effective field theories, we also provide the generalization of our many-body order parameters Eq. (2) and Eq. (3) by introducing many-body operators acting on subsystems rather than full systems. Although we mainly focus on the quadrupolar case, we remark that all the discussions here can be straightforwardly generalized to the octupolar and higher-polar cases.

A. Derivation of Effective Action: Multipolar Electromagnetism

We start from the effective responses for electric multipoles. First, the uniform monopole or charge density ρ in a spatial region $\mathcal{M}$ has the following response:

$$S_{eff} = \int d\tau \int_{\mathcal{M}} d^d r \ \rho V(\boldsymbol{r}) \tag{4}$$

Second, a single dipole at the site $\boldsymbol{r}$ with the polarization $\vec{P} = q\boldsymbol{d}$ has the following response:

$$\begin{aligned} S_{\rm dipole} &= \int d\tau \ q\Big[V(\boldsymbol{r}+\boldsymbol{d}) - V(\boldsymbol{r})\Big] \approx \int d\tau \ q\boldsymbol{d}\cdot\boldsymbol{\partial} V(\boldsymbol{r}) \\ &= \int d\tau \ \vec{P}\cdot\vec{E}. \end{aligned} \tag{5}$$

Hence, when there are uniform polarization density $\vec{P}$ over the area $\mathcal{M}$, we find

$$S_{eff} = \int d\tau \int_{\mathcal{M}} d^d r \ \vec{P}\cdot\vec{E}. \tag{6}$$

Third, a single quadrupole $Q_{xy} = qd^2$ at the site $\boldsymbol{r} = (x, y)$ (see FIG. 1 (c)) has the following response:

$$\begin{aligned} S_{\rm quadrupole} &= \int d\tau \ q\Big[V(x,y) - V(x+d,y) \\ &\qquad - V(x,y+d) + V(x+d,y+d)\Big] \\ &\approx \int d\tau \ qd^2 \partial_x\partial_y V(x,y) \\ &= \int d\tau \ \frac{Q_{xy}}{2}\Big[\partial_x E_y + \partial_y E_x\Big]. \end{aligned} \tag{7}$$

Thus, when there are uniform quadrupole density Q_{xy} over the area $\mathcal{M}$, we find

$$S_{eff} = \int d\tau \int_{\mathcal{M}} d^d r \ \frac{Q_{xy}}{2}\Big[\partial_x E_y + \partial_y E_x\Big], \tag{8}$$

which is the effective action for the quadrupole insulator.

It is straightforward to show that the uniform octupole density O_{xyz} over the region $\mathcal{M}$ has the following response:

$$S_{eff} = \int d\tau \int_{\mathcal{M}} d^d r \ \frac{O_{xyz}}{3}\Big[\partial_x\partial_y E_z + \partial_z\partial_y E_x + \partial_z\partial_x E_y\Big]. \tag{9}$$

B. From $\langle \mathbf{GS}|\hat{U}_a|\mathbf{GS}\rangle$ to Partition Functions

Here we relate the ground state overlaps and the partition functions, which has been extensively used in many-body order parameters for symmetry-protected topological states[9,10] on the relation of the ground state expectation values of the symmetry operators and the partition functions. Our approach is nothing but a small variation of the Dyson formula, which can be found in standard quantum field theory textbooks.

We first start by noting that

$$|\mathrm{GS}_\beta\rangle = \frac{1}{\sqrt{Z}}\sum_n e^{-\frac{\beta}{2}H}|n\rangle, \quad Z = \mathrm{Tr}[e^{-\beta H}], \tag{10}$$

where the true ground state $|\mathrm{GS}\rangle$ can be obtained by letting the "temperature" $1/\beta \to 0$. This implies that

$$\begin{aligned} \langle \mathrm{GS}_\beta|\hat{U}_a|\mathrm{GS}_\beta\rangle &\propto \frac{1}{Z}\sum_n \langle n|e^{-\frac{\beta}{2}H}\hat{U}_a e^{-\frac{\beta}{2}H}|n\rangle \\ &= \frac{1}{Z}\mathrm{Tr}\Big[e^{-\beta H}\hat{U}_a\Big]. \end{aligned} \tag{11}$$

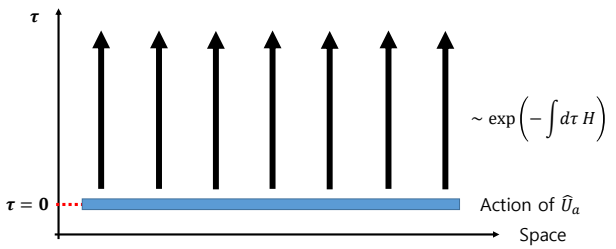

FIG. 2. Interpretation of partition functions with the insertion of $\hat{U}_a$. $\hat{U}_a$ acts at $\tau = 0$ followed by the imaginary time evolution along τ. Periodic boundary condition is used along τ direction.

Now, in order to relate Eq. (11) to the effective functional against the gauge potential configuration $A_{0;a}(\mathbf{r})$ set by $\hat{U}_a$, we need to properly interpret the partition function in the RHS of Eq. (11). Pictorially, this can be represented as the imaginary time evolution (See FIG. 2). For a proper interpretation, let us break the partition function into the two parts. The first part is the action of $\hat{U}_a$. Note that these $\hat{U}_a$'s involve complex phase factors proportional to the particle number, i.e., $\hat{U}_a \sim \exp\left[i\phi_a(\boldsymbol{r})\hat{n}(\boldsymbol{r})\right]$. This means that $\hat{U}_a$ appearing on the partition function Eq. (11) is the same as the action of the gauge potential $A_{0;a}(\boldsymbol{r},\tau)$ on the states at $\tau = 0$, i.e., $A_{0;a}(\boldsymbol{r},\tau) \propto \delta(\tau)$. In the second part, we act $\exp(-\beta H)$, which is the imaginary time-evolution on the states after the action of $\hat{U}_a$.

Because the RHS of Eq. (11) can be interpreted as the evolution of the states under the gauge potentials, the RHS should be equivalent to the following:

$$\langle \mathrm{GS}_\beta | \hat{U}_a | \mathrm{GS}_\beta \rangle \sim |Z| \exp\left(iS_{eff}[A_{0;a}(\boldsymbol{r},\tau)]\right), \qquad (12)$$

in which $S_{eff}[A_0(\boldsymbol{r},\tau)]$ is the effective response against $A_{0;a}(\boldsymbol{r},\tau)$, which is set by $\hat{U}_a$. Here, we also used the fact that the multipolar electromagnetic responses are *topological* (or Berry phase) because they involve a single time-derivative $\sim \partial_\tau$. Thus, this multipolar response against $A_{0;a}(\boldsymbol{r},\tau)$ contributes to the imaginary part of the $\langle \hat{U}_a \rangle$.

C. From Effective Field Theory to Corner Charge

We now relate the corner charge and effective field theory for quadrupole insulators Eq. (8) which justifies why our many-body order parameter Eq. (2) captures the corner charge originated from bulk quadrupole moment.

Let us begin with the well-known dipole case. Previously, we have derived

$$A_{0;a=1}(x,\tau) = 2\pi\frac{x}{L_x}\delta(\tau), \quad S_{eff} = \int_0^{L_x} dx \int_0^{\beta} d\tau \; P_x \cdot E_x$$

using the semi-classical electromagnetism response of the polarization $S_{eff} = \int \vec{P}\cdot\vec{E}$. Remarkably, despite of its semi-classical origin, we note that it is equivalent to the fully-quantum theory[23,24] of one-dimensional topological insulator. Explicitly evaluating the value of the effective action, we find $\langle \hat{U}_1 \rangle \propto e^{2\pi i P_x}$. This can be further identified with the edge charge, which we derive by solving the equation of motion $q_{\text{edge}} = \int dx \, \frac{\delta \mathcal{L}_{eff}}{\delta A_0} = P_x$.

For the quadrupole case, the effective response is

$$S_{eff} = \int_0^{\beta} d\tau \int_0^{L_x} dx \int_0^{L_y} dy \; \frac{Q_{xy}}{2}(\partial_y E_x + \partial_x E_y), \qquad (13)$$

where Q_{xy} is the physical quadrupole moment density and $E_{x,y}$ are electric fields. Implementing $A_{0;a=2} = \frac{2\pi}{L_x L_y} xy\delta(\tau)$, we find:

$$\langle \hat{U}_2 \rangle \propto e^{2\pi i Q_{xy}} \qquad (14)$$

It is straightforward to show that this quadrupole moment Q_{xy} is precisely the corner charge q_c, i.e., $Q_{xy} = q_c$, by solving the equation of motion for the probe gauge field δA_0 as done in the polarization case. Similar reasoning can be applied to the octupole case, too.

D. Corner Charge and Thouless Pumping

The effective theory Eq. (8) captures defining characteristics of the quadrupole insulator, the corner charge and the charge current pattern generated from an adiabatic Thouless pumping. To demonstrate these, let us consider a rectangular region $\mathcal{M} = (-L_x, L_x)\times(-L_y, L_y)$ with uniform $Q_{xy} \neq 0$, which has an open boundary with the vacuum $Q_{xy} = 0$ as described in Fig. 3 (a).

1. *Corner charge*

We first revisit the corner charge. It can be done by computing the equation of motion for A_0 in the effective response:

$$\rho(\boldsymbol{r}) = \frac{\delta \mathcal{L}_{eff}}{\delta A_0(\boldsymbol{r})} = \partial_x \partial_y Q_{xy} \qquad (15)$$

Obviously, the RHS of the above equation, $\partial_x\partial_y Q_{xy}$, is non-zero only at the corners of $\mathcal{M}$. Hence, we find

$$\rho(\boldsymbol{r}) = Q_{xy}\Big[\delta(x-L_x)\delta(y-L_y) - \delta(x+L_x)\delta(y-L_y) - \delta(x-L_x)\delta(y+L_y) + \delta(x+L_x)\delta(y+L_y)\Big]. \qquad (16)$$

This is consistent with the intuitive picture of the corner charge generated from the quadrupolar moment density.

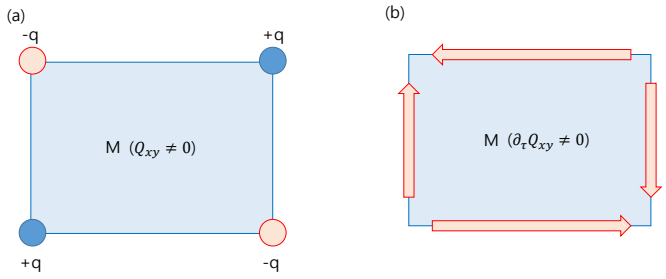

FIG. 3. (a) Corner charges of quadrupolar insulator derived from the effective action. Charges are only localized at four corners of the rectangular region $\mathcal{M}$, which has nonzero quadrupole moment $Q_{xy} \neq 0$. Note that the vacuum has trivial quadrupole moment $Q_{xy} = 0$. (b) Charge current configuration derived from the effective action under the Thouless pumping. In this case, charges flow only along the boundary of $\mathcal{M}$ and their directions are denoted as arrows.

Integrating over the quadrant of the $\mathcal{M}$, we finally find that

$$q_c = \pm Q_{xy}, \tag{17}$$

whose sign depends on which quadrant of the space that we integrate over.

2. *Thouless pumping*

Next we imagine that the uniform quadrupolar moment density Q_{xy} depends on time, i.e., we have $Q_{xy} = Q_{xy}(\tau)$. This allows the charge currents to flow along the boundary of the topological quadrupolar insulators. To see this, we calculate

$$J_x = \frac{\delta \mathcal{L}_{eff}}{\delta A_x} = -\partial_y \partial_\tau Q_{xy}, \quad J_y = \frac{\delta \mathcal{L}_{eff}}{\delta A_y} = -\partial_x \partial_\tau Q_{xy}, \tag{18}$$

which is essentially equivalent to the charge flow in the process of Thouless pumping in the topological quadrupolar insulator, obtained in Ref. [12]. See FIG. 3 (b) for the direction of current along the boundary of $\mathcal{M}$ during the Thouless pumping.

In summary, within the effective field theory approach using semi-classical electromagnetic responses, our many-body order parameters applied to fully quantum systems would capture the corner charges q_c, i.e., $\langle \hat{U}_a \rangle \approx \exp(2\pi i q_c), a = 1, 2, 3$, which are the physical manifestation of the multipole moments even in the absence of any quantizing symmetries.

E. Generalizations of Many-Body Order Parameters

With the effective theory in hand, we can now generalize our order parameters to arbitrary boundary condition, since the (semi-classical) relation Eq. (14) holds independently of which boundary condition being used. Furthermore, we can generalize the unitary $\hat{U}_a$ to other unitaries saturating the effective action. For example, we can use

$$\hat{V}_1(l) = \begin{cases} \exp\left[\frac{2\pi i}{l} \sum_x x \hat{n}(x)\right] & \text{for } x \in (0, l] \\ 1 & \text{for } x \in (l, L_x], \end{cases} \tag{19}$$

to measure the polarization.[25] Here the whole system may be subject to the open boundary condition or to the periodic boundary condition. Similarly, we can define the generalized measure for the quadrupole moment as follows:

$$\hat{V}_2(l) = \begin{cases} \exp\left[\frac{2\pi i}{l^2} \sum_{\boldsymbol{r}} xy \hat{n}(\boldsymbol{r})\right] & \text{for } \boldsymbol{r} \in (0, l] \times (0, l] \\ 1 & \text{otherwise.} \end{cases} \tag{20}$$

Again, the whole system may be subject to the periodic or open boundary conditions.

IV. NUMERICAL DEMONSTRATION OF MANY-BODY ORDER PARAMETERS

We now proceed to the numerical demonstration for our many-body order parameters by testing the formula on the *non-interacting* topological quadrupolar states. We emphasize here again that, though the models are non-interacting, the quantity that we are computing is intrinsically a many-body quantity which requires the full knowledge of the many-body ground state.

A. Topological Quadrupole Insulators

In the momentum basis, the Hamiltonian for a topological quadrupole insulator[12] is

$$\begin{aligned} h(\boldsymbol{k}) =& \big(\gamma_x + \lambda_x \cos(k_x)\big)\Gamma_4 + \lambda_x \sin(k_x)\Gamma_3 \\ &+ \big(\gamma_y + \lambda_y \cos(k_y)\big)\Gamma_2 + \lambda_y \sin(k_y)\Gamma_1 + \delta\ \Gamma_0. \end{aligned} \tag{21}$$

Here, $\Gamma_{a=0,\cdots,4}$ is a proper set of gamma matrices. When $\delta = 0$, there are two anti-commuting mirror symmetries $\hat{M}_x$ and $\hat{M}_y$ which quantize the quadrupole moment Q_{xy} to either 0 or 1/2 mod 1. If $\lambda_x = \lambda_y$ and $\gamma_x = \gamma_y$ are imposed (while keeping $\delta = 0$), there is an additional $\hat{C}_4$ symmetry which also quantizes the quadrupole moment Q_{xy} to either 0 or 1/2 mod 1. Introduction of $\delta \neq 0$ breaks both the mirror symmetries and $\hat{C}_4$ symmetry, which quantize the quadrupoles, but $\hat{C}_2$ symmetry remains intact which enforce the total polarization to vanish.

In FIG. 4 (b) and (c), we present how the complex phase of $\langle \hat{U}_2 \rangle$ changes along different cuts in the parameter space of Eq. (21) as described in FIG. 4 (a). The

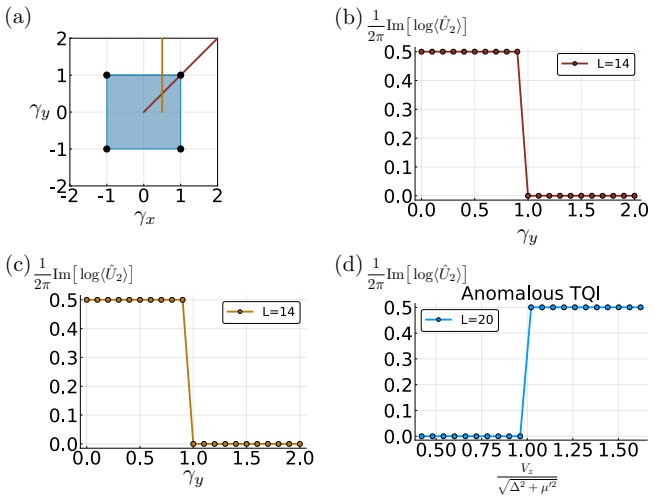

FIG. 4. (a) The phase diagram of the quadrupole insulator Eq. (21) when $\delta = 0$ and $\lambda_x = \lambda_y = 1$. The shaded region denotes topologically nontrivial phase (quadrupole moment equals 0.5) and black dots denote bulk energy gap closing points. (b) and (c) are evaluation of Q_{xy} Eq. (2) for the quadrupole insulator Eq. (21). We set $\lambda_x = \lambda_y = 1$ and $\delta = 0$, and evaluate Q_{xy} (b) along the cut $\gamma_x = \gamma_y$ and (c) along the cut $\gamma_x = 0.5$. We see in both cases there is a sharp change at $\gamma_y = 1$, which is consistent with the phase diagram (a). (d) Anomalous topological quadrupole insulator.[19] Here, the ground state is known to be topological if $\frac{V_z}{\sqrt{\Delta^2+\mu'^2}} > 1$ and trivial if $\frac{V_z}{\sqrt{\Delta^2+\mu'^2}} < 1$, and this is well captured by $\hat{U}_2$. See the main text for details on the model and the numerical values of the parameters.

many-body order parameter Eq. (2) reproduces the quantized quadrupole moments as well as the sharp phase transitions between topological and trivial quadrupole insulator, even when the bulk energy gap does not close at the transition point.

To define the quadrupole moment using the nested Wilson loop, the existence of the Wannier gap is crucial as we can then separate a Wannier band to evaluate the Wanner-sector polarization. In the case of Eq. (21) with $\delta = 0$, the phase transition between topological and trivial quadrupole insulator happens when the Wannier gap (instead of physical energy gap) closes and re-opens. On the other hand, $|\langle\hat{U}_2\rangle|$ always vanishes at phase boundary, where the Wannier gap closes i.e., $|\lambda_x/\gamma_x| = 1$ *or* $|\lambda_y/\gamma_y| = 1$ (Note that the energy gap closes only when $|\lambda_x/\gamma_x| = 1$ *and* $|\lambda_y/\gamma_y| = 1$). This highlights the relation between the Wannier gap and $|\langle\hat{U}_2\rangle|$.

B. Anomalous Topological Quadrupolar Insulator

Given the success of our many-body formula in reproducing the phase diagram of Eq. (21), we apply it to the anomalous topological quadrupole insulator,[19] where the naive application of the nested Wilson loop approach fails to predict the non-zero quantized quadrupole moments and the related phase transition.

A minimal model for an anomalous topological quadrupole insulator is given by Ref. [19]

$$\begin{aligned} H_{\mathrm{ATQI}}(\mathbf{k}) =& \big[2t_x\big(1-\cos(k_x)\big)-\mu\big]\sigma_3\otimes\sigma_0\otimes\sigma_0 \\ &+ V_z\sigma_0\otimes\sigma_3\otimes\sigma_0 + \Delta\sigma_1\otimes\sigma_0\otimes\sigma_0 \\ &+ \alpha\sin(k_x)\sigma_3\otimes\sigma_2\otimes\sigma_0 \\ &- \big[\beta_1-\beta_2\cos(k_y)\big]\sigma_3\otimes\sigma_1\otimes\sigma_2 \\ &- \beta_2\sin(k_y)\sigma_3\otimes\sigma_1\otimes\sigma_1, \end{aligned} \tag{22}$$

where t_x is the nearest neighbor hopping strength in x-direction, μ is the chemical potential, V_z is the Zeeman energy, Δ is the superconducting pairing strength, α and β_1/β_2 are the Rashba spin-orbit coupling strengths in x- and y-direction. In FIG. 4 (d), we set $(t_x, \mu, \Delta, \alpha, \beta_1, \beta_2) = (1.7, -0.9, 1.6, 3.7, 0.8, 6.2)$ and tune $V_z \in [0.7, 2.7]$ following Ref. [19]. When $V_z > \sqrt{\Delta^2+\mu'^2}$, the half-filled ground state is topologically nontrivial and when $V_z < \sqrt{\Delta^2+\mu'^2}$, the half-filled ground state is trivial where $\mu' \approx 0.46$ for our choices of parameters. As can be seen in FIG. 4 (d), we find remarkably that both the expected quadrupole moment and phase transition are successfully reproduced with our many-body order parameter Eq. (2).

C. Topological Octupolar Insulator

A minimal model for an octupole insulator is given by[12]

$$\begin{aligned} h_{\mathrm{octupole}}(\mathbf{k}) =& \lambda_y\sin(k_y)\Gamma'_1 + \big[\gamma_y+\lambda_y\cos(k_y)\big]\Gamma'_2 \\ &+ \lambda_x\sin(k_x)\Gamma'_3 + \big[\gamma_x+\lambda_x\cos(k_x)\big]\Gamma'_4 \\ &+ \lambda_z\sin(k_z)\Gamma'_5 + \big[\gamma_z+\lambda_z\cos(k_z)\big]\Gamma'_6, \end{aligned} \tag{23}$$

where $\Gamma'_i = \sigma_3\otimes\Gamma_i$ for $i = 0,1,2,3$ with Γ_i being the same set of Gamma matrices appearing in Eq. (21), $\Gamma'_4 = \sigma_1\otimes I_{4\times4}$, $\Gamma'_5 = \sigma_2\otimes I_{4\times4}$, $\Gamma'_6 = i\Gamma'_0\Gamma'_1\Gamma'_2\Gamma'_3\Gamma'_4\Gamma'_5$, and $\gamma_{x,y,z}$ and $\lambda_{x,y,z}$ are intra- and inter-site hopping strengths. When $|\lambda_i| > |\gamma_i|$ for all $i = x, y, z$, the half-filled ground state has topologically nontrivial octupole moment.

We present the numerical evaluation of the expectation value of $\hat{U}_3$ with respect to the half-filled ground state of the octupole insulator Eq. (23). As done in the quadrupole insulator case [FIG. 4 (a)], we see that the complex phase of $\langle\hat{U}_3\rangle$ correctly captures the topological and trivial phases as the parameter passes through the phase transition between the topological octupole insulator and the trivial insulator [FIG. 5 (a)].

D. Edge-Localized Polarization Model

One of the key characteristic of the tight-binding quadrupole insulator model Eq. (21) is that the following

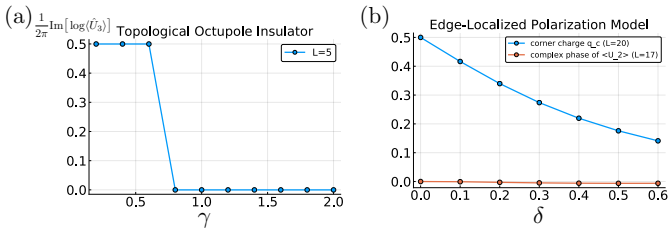

FIG. 5. (a) The complex phase of $\langle \hat{U}_3 \rangle$ for topological octupole insulator Eq. (23). We set $\lambda_x = \lambda_y = \lambda_z = 1.0$ and tune $\gamma \equiv \gamma_x = \gamma_y = \gamma_z \in [0, 2]$. When $\gamma < 1.0$ ($\gamma > 1.0$), the ground state is in topological (trivial) octupole insulator phase, which is indeed captured by $\langle \hat{U}_3 \rangle$ up to finite-size effect. (b) Edge-localized polarization model Eq. (24) with $(\gamma, \lambda_x, \lambda_y) = (0.1, 1.0, 0.5)$ and change $\delta \in [0, 0.6]$. The corner charge comes solely from the boundary localized polarization and the bulk quadrupole moment vanishes. We indeed see that the complex phase of $\langle \hat{U}_2 \rangle$ is trivial up to finite size effects.

four physical observables are identical even when $\delta \neq 0$: $q_c = |p_x^{\rm edge}| = |p_y^{\rm edge}| = Q_{xy}$, where q_c is the corner charge localized at one edge in the case of full open boundary condition, $p_{x(,y)}^{\rm edge}$ is edge localized polarization along x-direction (y-direction) in the case of open boundary condition along x-direction (y-direction) and periodic boundary condition along y-direction (x-direction), and Q_{xy} is the bulk quadrupole moment. In contrast, there exists model, *edge-localized polarization* model, in which $q_c = |p_x^{\rm edge}| + |p_y^{\rm edge}|$ and $Q_{xy} = 0$ instead. A minimal model for this edge-localized polarization model is given by[12]

$$h(\mathbf{k}) = \begin{pmatrix} \delta\tau_0 & q(\mathbf{k}) \\ q^\dagger(\mathbf{k}) & -\delta\tau_0 \end{pmatrix},$$
$$q(\mathbf{k}) = \begin{pmatrix} \gamma + \lambda_x e^{ik_x} & \gamma + \lambda_y e^{ik_y} \\ \gamma + \lambda_y e^{-ik_y} & \gamma + \lambda_x e^{-ik_x} \end{pmatrix}, \qquad (24)$$

where τ_0 is the 2×2 identity matrix and γ and λ are intra- and inter-layer hopping strengths. To see our many-body order parameter Eq. (2) in terms of $\hat{U}_2$ indeed not sensitive to the edge-localized polarization that is not coming from the bulk quadrupole moment, we numerically compute the complex phase of $\langle \hat{U}_2 \rangle$ for the minimal model Eq. (24). In FIG. 5 (b), we set $(\gamma, \lambda_x, \lambda_y) = (0.1, 1.0, 0.5)$ and change $\delta \in [0, 0.3]$. As we tune δ, the corner charge changes and equals $|p_x^{\rm edge}| + |p_y^{\rm edge}|$, while the bulk quadrupole moment vanishes. As can be seen in the figure, the complex phase of $\langle \hat{U}_2 \rangle$ is negligible, hence capturing the vanishing bulk quadrupole moment.

E. Generalized Many-Body Order Parameters

We perform the numerical check for the generalized many-body order parameters Eq. (19) and Eq. (20), which is presented in FIG. 6. We compute the phases

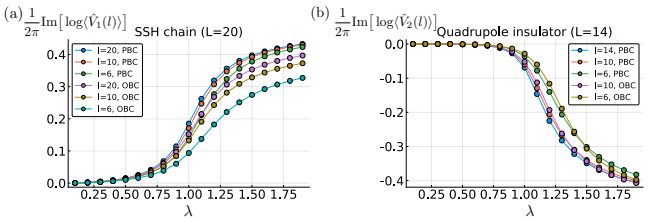

FIG. 6. Evaluation of the phase of $\langle \hat{V}_{a=1,2}(l) \rangle$ of Eq. (19) and Eq. (20) for various values of l in the case of (a) Su-Schrieffer-Heeger chain Eq. (25) and (b) Quadrupole insulator Eq. (21). We set $\gamma = 1.0$ ($\gamma_x = \gamma_y = 1.0$) and $\delta = 0.2$ and change λ ($= \lambda_x = \lambda_y$).

of these order parameters for various l's for the Su-Schrieffer-Heeger chain[26] and topological quadrupolar insulators Eq. (21), which are both subject to the nonzero δ that breaks the quantization of polarization and quadrupole moments. For the Su-Schrieffer-Heeger chain, we used

$$h_{\rm SSH}(k) = \begin{pmatrix} \delta & \gamma + \lambda e^{-ik} \\ \gamma + \lambda e^{ik} & -\delta \end{pmatrix}. \qquad (25)$$

Surprisingly, the overall trend is insensitive to which boundary condition is used and insensitive even when l is less than a half of the system size. Remarkably when $\delta = 0$, i.e., the bulk multipole moment is quantized, and when the periodic boundary condition is used, we have confirmed numerically that (at least up to the system size $L \sim 20$) the generalized many-body order parameters Eq. (19) and Eq. (20) reproduce the original many-body order parameters Eq. (1) and Eq. (2) even when l is an order of the half of the system size [please refer to Appendix D 2 a for more details].

V. BULK-BOUNDARY CORRESPONDENCE AND THOULESS PUMPING

A. Corner Charge, Nested Wilson Loop Quadrupole Moment, and Physical Quadrupole Moment

Here we discuss a few related but distinct quantities when the symmetries quantizing the multipole moments are lost, by restricting ourselves to the quadrupolar case. (1) corner charge q_c, which is the total electric charge near the corner when the system is subject to the open boundary conditions. (2) Wannier-sector polarizations[12] $\{p_x^\omega, p_y^\omega\}$ (when they can be defined) and associated "nested Wilson loop quadrupole moment" $Q_{xy}^\omega = 2p_x^\omega p_y^\omega$, which are defined by nested Wilson loops, and (3) physical quadrupole moment $Q_{xy}^{\rm ph}$. In general, all these three can be different from each other.

However, if the bulk and boundary-alone polarizations are absent (so that the quadrupole moments are well-defined) and if the quadrupolar charge distribution per

unit cell is the only source of the corner charge, then the corner charge q_c would agree with a sensible quadrupole moment $Q_{xy}^{\rm ph}$.[12]

In general, if we assume the strongest form of the bulk-boundary correspondence,[11,12,27,28] we expect

$$Q_{xy}^{\rm ph} = p_x^{\rm edge} + p_y^{\rm edge} - q_{\rm c} \ (\mathrm{mod}\ 1), \tag{26}$$

where $p_x^{\rm edge}$ and $p_y^{\rm edge}$ are edge-localized polarizations along x-and y-directions, even in the absence of quantizing symmetries. We note that this form of the bulk-boundary correspondence is insensitive to dressing polarization chains along the open boundaries. When the boundary polarization of the systems of the open boundary condition is fully determined by the bulk quadrupole moments,[12] the bulk-boundary correspondence reduces to $Q_{xy}^{\rm ph} = q_c$.

In the remaining section, we would like to see to what extent our many-body order parameter Q_{xy}, which is the complex phase factor of the expectation value of $\hat{U}_2$, can capture the physical bulk quadrupole moment for the cases where the gap in the nested Wilson loop spectrum is present (i.e., Q_{xy}^{ω} can be defined).[12] We will see that, at least for the examples that we considered below, Q_{xy} *reproduces the bulk quadrupole moment* $Q_{xy}^{\rm ph}$, while Q_{xy}^{ω} cannot, *in the absence of quantizing symmetries.*

We would like to comment that the nested Wilson loop quadrupole moment Q_{xy}^{ω} is originally designed as "topological index" with quantizing crystalline symmetries.[11,12] Hence, once the quantizing symmetries are relaxed, the nested Wilson loop quadrupole moment Q_{xy}^{ω} may not agree with the physical quadrupole moment $Q_{xy}^{\rm ph}$ as already exposed in [12]. See the detailed discussion and explanation on this point in [12]. Indeed, in the presence of quantizing symmetries, we consistently find that Q_{xy}^{ω} does serve both as the index and also the physical measure of the quadrupole moment.

B. Thouless Pumping

1. *Topological Quadrupole Insulator with π-flux per Plaquette*

In this section, we consider one of the first tight-binding model for the quadrupole insulator[12] which has π-flux per plaquette. In the momentum basis, the explicit form of the Hamiltonian is presented in Eq. (21). As previously mentioned, $\delta \neq 0$ breaks both the mirror symmetries and $\hat{C}_4$ symmetry, which quantize the quadrupoles, but $\hat{C}_2$ symmetry remains intact which enforces the total polarization to vanish. We now ask what would happen if we break symmetries that protect the quantization of the quadrupole moment by introducing non-zero δ. In this case, the quantization of the quadrupole moment is lost and the quadrupole moment can take any value. However, due to the bulk-boundary correspondence,[12,27,28] we expect that the corner charge is still determined by the bulk quadrupole moment.

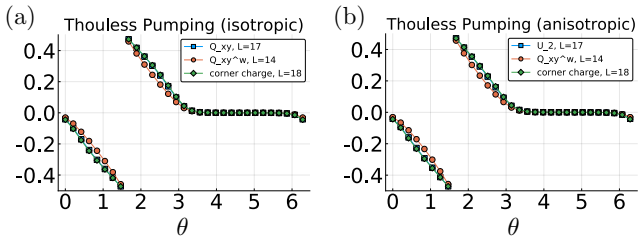

FIG. 7. Comparison between three different physical quantities, complex phase of $\langle \hat{U}_2 \rangle$, the nested Wilson quadrupole moment Q_{xy}^{ω}, and corner charge $q_{\rm c}$ for (a) isotropic Thouless pumping Eq. (27) and (b) anisotropic Thouless pumping Eq. (28). While the complex phase of $\langle \hat{U}_2 \rangle$ and the corner charge $q_{\rm c}$ agree with each other with almost no discernible differences, Q_{xy}^{ω} given in terms of the Wannier-sector polarizations agrees with the two only at $\theta = \pi/2, 3\pi/2$, i.e., $\delta = 0$ and the quadrupole moment is quantized.

We employ two Thouless pumping processes, one we call isotropic Thouless process and the other we call anisotropic Thouless process, where we relate three different quantities; a) the complex phase factor of $\langle \hat{U}_2 \rangle$ evaluated under full periodic boundary condition, b) the nested Wilson quadrupole moment[12] $Q_{xy}^{\omega} = 2p_x^{\omega}p_y^{\omega}$ obtained from the nested Wilson loop, and c) the corner charge $q_{\rm c}$ localized at one corner under full open boundary condition. We note that the previous study[12] found numerically that b) and c) are not equivalent in the absence of the quantizing symmetries.

For the isotropic Thouless pumping case, we change the parameters in Eq. (21) according to

$$\begin{cases} \gamma_x = \gamma_y = 1 - 0.6\sin(\theta) \\ \lambda_x = \lambda_y = 1 + 0.6\sin(\theta) \\ \delta = 0.6\cos(\theta) \end{cases}, \tag{27}$$

and for the anisotropic Thouless pumping process, we change the parameters according to

$$\begin{cases} \gamma_x = 1 - 0.6\sin(\theta), \quad \gamma_y = 1 - 0.5\sin(\theta) \\ \lambda_x = 1 + 0.6\sin(\theta), \quad \lambda_y = 1 + 0.5\sin(\theta) \\ \delta = 0.6\cos(\theta) \end{cases}, \tag{28}$$

where $\theta \in [0, 2\pi]$ is the pumping parameter. In FIG. 7, we have plotted the three fundamentally different physical quantities for (a) isotropic and (b) anisotropic Thouless pumping processes. From the plots, we see almost no discernible difference between the complex phase factor of $\langle \hat{U}_2 \rangle$ and the corner charge $q_{\rm c}$, indicating that the many-body order parameter faithfully represents the physical quadrupole moment during two Thouless processes. Since the edge localized polarizations $p_x^{\rm edge}$ and $p_y^{\rm edge}$ are equal to corner charge $q_{\rm c}$ during the Thouless processes (data not shown), we see that $\hat{U}_2$ does precisely measure the physical quadrupole moment. We also note that the Wilson loop quadrupole moment Q_{xy}^{ω} differs from the two in general and agrees with the two only at quantized values.

2. *Topological Quadrupole Insulator with $\pi/2$-flux per Plaquette*

In this section, we present an example where the bulk quadrupole moment is not the only source for the corner charge, hence providing a nontrivial test of whether our many-body order parameter using $\hat{U}_2$ reproduce the exact numerical value of the bulk (physical) quadrupole moment when the quantizing symmetries are lost.[29] Let us begin with a topological quadrupole insulator with $\pi/2$-flux on every plaquette, which is described in FIG. 8 (a). Because of the mirror symmetries (or $\hat{C}_4$ symmetry in the isotropic case), when the inter-site hoping strengths are larger than intra-site hopping strengths, the half-filled ground state is in topological quadrupole insulator phase where both the nested Wilson loop quadrupole moment and the expectation value of many-body order parameter $\hat{U}_2$ give quadrupole moment 0.5. We now introduce onsite potential terms $\delta \sum_{\mathbf{r}} \left(c^\dagger_{\mathbf{r},1}c_{\mathbf{r},1} + c^\dagger_{\mathbf{r},2}c_{\mathbf{r},2} - c^\dagger_{\mathbf{r},3}c_{\mathbf{r},3} - c^\dagger_{\mathbf{r},4}c_{\mathbf{r},4}\right)$ which explicitly breaks mirror symmetries (and $\hat{C}_4$ symmetry) but preserving $\hat{C}_2$ symmetry.

Finally, we consider the following Thouless pumping process:

$$\begin{cases} \gamma_x = \gamma_y = 1 - 0.6\sin(\theta) \\ \lambda_x = \lambda_y = 1 + 0.6\sin(\theta) \\ \delta = 0.6\cos(\theta) \end{cases}, \tag{29}$$

where $\theta \in [0, 2\pi)$ is the pumping parameter. In FIG. 8 (b), we show how (i) the many-body order parameter in terms of $\hat{U}_2$ under periodic boundary condition, (ii) the many-body order parameter in terms of $\hat{U}_2$ under open boundary condition, (iii) physical quadrupole moment Q^{ph}_{xy} by assuming the bulk boundary correspondences Eq (26), i.e., $p^{\mathrm{edge}}_x + p^{\mathrm{edge}}_y - q_{\mathrm{c}}$, and (iv) the corner charge q_{c} change during the Thouless pumping process. Note that in this model (iii), the non zero physical quadrupole moment, is not the only source for (iv), the corner charge.

Apparent from the plot, the many-body order parameter using $\hat{U}_2$ with respect to the periodic boundary condition does exactly reproduce the precise numerical value of the physical quadrupole moment during the Thouless pumping process. Furthermore, the many-body order parameter with respect to the open boundary condition seems to reproduce the corner charge exactly. To see whether the many-body order parameter using $\hat{U}_2$ with respect to the open boundary condition indeed reproduce the corner charge, in FIG. 8 (c) we computed the system size dependence at $\theta = \pi/4$ in Eq. (29) at which the difference between the corner charge and the bulk quadrupole moment becomes large. As we can see from the plot, the many-body order parameter using $\hat{U}_2$ with respect to the open boundary condition indeed approaches to the corner charge in the thermodynamic limit. We plan to discuss how $\langle \hat{U}_2 \rangle$ with respect to the states under open boundary condition measures the corner charge using the effective field theory in the future work.[30]

VI. CONCLUSIONS

We have proposed many-body order parameters which measure quantized bulk multipoles in crystalline many-body quantum states. We provided numerical illustration of our order parameters by presenting explicit computations in toy models and confirmed that if the multipole moment can be defined via the nested Wilson loop, they can measure the bulk multipole moments even when there does not exist symmetries quantizing the bulk multipole moments. Using analytical arguments, we also have demonstrated that they capture the corner charges originating from the bulk multipole moments. Based on the reasonings of the effective field theories, we have provided an extension of our formulas, which work even for the case of open boundary condition.

Now let us discuss a few non-trivial tests of our formula. First, we confirmed that our many-body order parameter can diagnose the non-trivial topology of a bosonic higher-order topological insulator with corner spin at an exactly soluble point,[31,32] which is explained in Appendix B. Second, we also have applied our order parameter Eq. (2) to the "edge-localized polarization model"[12] which supports quantized corner charges $q_c = \pm 1/2$ yet having vanishing quadrupole moment (with suitable perturbations). In this case as well, our order parameter correctly captures the vanishing quadrupole moment despite of the nonzero corner charges coming from edge-alone polarizations. We would also like to mention the application of our formula to the amorphous systems[33] and sonic crystals:[34] in both cases the many-body order parameter Eq. (2) can diagnose the quadrupole moments correctly and reproduce the phase diagrams.

Next we comment on the applicability of our formula Eq. (2) for the cases without a gap in the Wilson loop spectrum, e.g., some C_4-symmetric models in Ref. 20 and models in Ref. 35. Because the Wannier band is gapless in these cases, quadrupole moment cannot be defined within the nested Wilson loop scheme. Given that we have constructed the many-body order parameters for the multipoles originating from the nested Wilson loop topology, we expect that $\langle \hat{U}_2 \rangle$ neither detect the higher-order topology of these models nor give any sensible values. Indeed, we find that our formula Eq. (2) does not show stable values against the continuous change in parameters for these cases as demonstrated in Appndix E. This is in fact consistent with the observation made in Ref. 35, where some anomalous behavior of $\langle \hat{U}_2 \rangle$ on the C_4-symmetric models was discussed. We would like to mention that the coordinate dependence of our many-body order parameter, which is extensively discussed in Appendix D 2 b, is again consistent with the observation made in Ref. 35 regarding the "choice of coordinate" in $\hat{U}_2$.

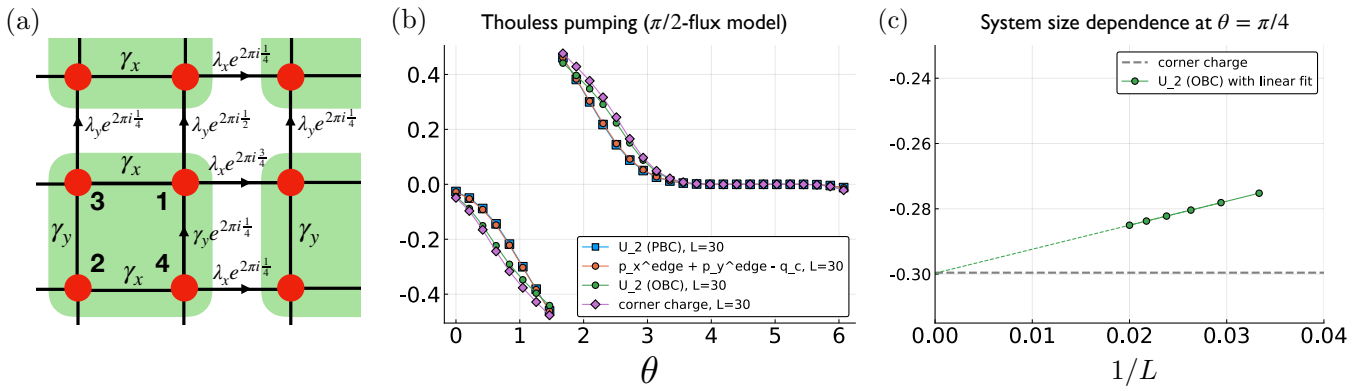

FIG. 8. (a) Tight binding model of topological quadrupole insulator with $\pi/2$-flux per unit cell. The tight binding hopping parameters are shown in the figure with arrows which specify the direction of the hopping. (b) Comparison between several different physical quantities, the many-body order parameter Q_{xy} using $\langle \hat{U}_2 \rangle$ with respect to periodic and open boundary condition, the physical quadrupole moment via the bulk-boundary correspondence Eq. (26) $p_x^{\rm edge} + p_y^{\rm edge} - q_c$, and corner charge q_c during the Thouless pumping Eq. (29). We see a remarkable agreement between the many-body order parameter Q_{xy} using $\hat{U}_2$ under periodic boundary condition and the physical quadrupole moment. The many-body order parameter Q_{xy} using $\hat{U}_2$ under open boundary condition agrees with the corner charge q_c up to finite size error. (c) The system size dependence of the many-body order parameter Q_{xy} using $\hat{U}_2$ under open boundary condition at $\theta = \pi/4$ in Eq. (29) and the convergence to the corner charge in the thermodynamic limit.

When the symmetries quantizing the multipole moment are lost, the bulk multipole moment can take arbitrary value and so does the corner charge. However, If we assume the strongest form of the bulk-boundary correspondence,[11,12,27,28] for bulk quadrupole moment $Q_{xy}^{\rm ph} = p_x^{\rm edge} + p_y^{\rm edge} - q_c \pmod 1$ should hold, where $p_x^{\rm edge}$ and $p_y^{\rm edge}$ are the edge localized polarization along x- and y-directions and q_c is the corner charge. We expect similar relations to hold for octupole and higher multipole moments. This form of bulk-boundary correspondence is especially insensitive to dressing polarization chains along open boundaries. We tested whether our many-body order parameter does satisfy the bulk-boundary correspondence in the absence of quantizing symmetries. While the nested Wilson quadrupole moment Q_{xy}^{ω} fails to capture the precise numeric value of the physical quadrupole moment $Q_{xy}^{\rm ph}$, our many-body order parameter Q_{xy} in Eq. (2) under periodic boundary condition agrees with $Q_{xy}^{\rm ph}$ during the Thouless processes. (Note again that Q_{xy}^{ω} agrees with $Q_{xy}^{\rm ph}$ when the quantizing symmetries present and this is consistent with the references[11,12] that the nested Wilson quadrupole moment serves as the topological band index of quantized quadrupole moment.) Therefore, we confirm that Q_{xy} under periodic boundary condition does reproduce the physical quadrupole moment. Interestingly, Q_{xy} under open boundary condition reproduces the corner charge, where the latter is originated from not only the physical quadrupole moment but also edge localized polarizations.[30]

In conclusion, we find that, when applied to the models with the Wilson loop gap and thus with the well-defined quadrupole moments, our many-body order parameters can measure the bulk multipole moments faithfully when quantizing symmetries are present or lost as extensively tested in various models.[12,33,34,36] To "prove" our proposal for the multipoles, there are several important questions to be addressed in the future. First, the detailed understanding of our many-body order parameters for the models without the Wannier gap is desirable. Second, the precise relation of our order parameter with nested Wilson loop indices will deepen our understandings of electric multipoles. Lastly, our order parameters, when compared with Resta's original proposal,[5] lack the periodicity in coordinates. We plan to discuss its implication in the future work.

ACKNOWLEDGMENTS

We thank Akira Furusaki, Jung Hoon Han, Hyun Woong Kwon, Joel E. Moore, Masaki Oshikawa, Kwon Park, Shinsei Ryu, and Mike Zaletel for helpful discussions and comments. KS is supported by PRESTO, JST (JPMJPR18L4) and GYC is supported by BK 21 plus program at POSTECH in Korea. GYC thanks KIAS in Korea and RIKEN in Japan for their hospitality where some part of this work has been done. We thank Taylor Hughes for informing us about their parallel independent work[36] and sharing it with us before uploading to arXiv. Whenever their work and our work overlap, the results agree with each other. We also thank Andrei Bernevig and Ben Wieder for their comments and explanation on nested Wilson loop indices. We are very grateful to the anonymous referee of this manuscript for his/her constructive comments and questions.

Appendix A: Details on Symmetry Properties of $\hat{U}_2$

In this section, we present the details of the symmetry actions on the many-body order operator $\hat{U}_2$ Eq. (2). This highlights under what conditions $\hat{U}_2$ is well-defined and yields a quantized value when evaluated with respect to a many-body state. In the following, we discuss the action of the crystalline $\hat{C}_4$ symmetry on the many-body order parameter and the large translation symmetry.

1. Large Translation Symmetry

Here we provide the details of the large coordinate translation operation $x \to x + L_x$ (with L_x being the system size along x-direction) on the many-body quadrupolar order parameter Eq. (2). As noted in the main text, we find

$$x \to x + L_x : \quad \hat{U}_2 \to \hat{U}_2 \hat{U}_{1;y} \tag{A1}$$

where $\hat{U}_{1;y}$ is the many-body measure for the polarization along y direction. Now the key step that we used in the main text was

$$\begin{aligned} \langle \hat{U}_2 \rangle &= \langle \hat{U}_2 \rangle \langle \hat{U}_{1;y} \rangle + \mathcal{O}\Big(\frac{\epsilon_0}{E_{\text{gap}}}\Big), \\ &= \langle \hat{U}_2 \rangle \langle \hat{U}_{1;y} \rangle + \mathcal{O}\Big(\frac{\xi}{a_0}\Big), \end{aligned} \tag{A2}$$

where ϵ_0 and a_0 are the unit energy and unit length scale which make the expressions dimensionless. From the first line to the second line, we used the fact that $\frac{1}{E_{\text{gap}}} \propto \xi$ with ξ being the correlation length. When the correlation length becomes an atomic scale $\xi \to 0^+$ (ultra-short correlated), i.e., the ideal atomic insulator limit, we see that $\langle \hat{U}_2 \rangle = \langle \hat{U}_2 \rangle \langle \hat{U}_{1;y} \rangle$ which enforces $\langle \hat{U}_{1;y} \rangle = 1$.

The above equations can be derived from the following observation:

$$\hat{U}_{1;y}|GS\rangle = \langle \hat{U}_{1;y} \rangle |GS\rangle + \mathcal{O}\Big(\frac{\epsilon_0}{E_{\text{gap}}}\Big), \tag{A3}$$

which is a slight rewriting of Eq. (37) in Ref. [22]. The same results hold for $\hat{U}_{1;x}$.

2. $\hat{C}_4$ Symmetry and Mirror Symmetries

With the discussion above, we now discuss the action of $\hat{C}_4$ on $\hat{U}_2$ for the domain $\mathcal{M} = (0, L_x] \times (0, L_y]$. Obviously the system respects the $\hat{C}_4$ symmetry only when $L_x = L_y = L$. Furthermore, the domain $\mathcal{M} = (0, L] \times (0, L]$ is transformed into $\mathcal{M}' = [-L, 0) \times (0, L]$ under $\hat{C}_4$. Hence, we find that

$$\hat{C}_4 : \hat{U}_2 \to \hat{U}_2^* \hat{U}_{1;x}. \tag{A4}$$

Since, in the ideal limit $\xi \to 0^+$, $\langle \hat{U}_2^* \hat{U}_{1;x} \rangle = \langle \hat{U}_2^* \rangle \langle \hat{U}_{1;x} \rangle = \langle \hat{U}_2^* \rangle$ (with vanishing polarization) and thus $\langle \hat{U}_2 \rangle = \langle \hat{U}_2^* \rangle$, this enforces $Q_{xy} = -Q_{xy}$ which is consistent with the previous work.[11] In fact, even for the mirror symmetries $\hat{M}_x \times \hat{M}_y$ discussed in the main text, extra factors of $\hat{U}_{1;\mu=x,y}$'s do show up, because of the transformations on the domain $\mathcal{M}$, which is to be included. Nevertheless, the conclusion made in the main text remains the same, i.e., $\hat{C}_4$ or mirrors flip the sign of Q_{xy}, which can be explicitly seen in our many-body order parameters in an appropriate limit.

Appendix B: Exactly-Solvable Bosonic Higher-Order Topological Insulator

Here we prove that our many-body order parameter can diagnose the bosonic higher-order topological insulator[31] at the exactly-solvable points, i.e., where the correlation length is the size of the unit cell. The model that we study here has four spin-$\frac{1}{2}$'s per unit cell and it consists of the two-spin interactions respecting $SU(2)$.

$$H = J \sum_{\text{P}} \sum_{\langle i,j \rangle \in \text{P}} \hat{S}_i \cdot \hat{S}_j + \lambda \sum_{\boldsymbol{R}} \sum_{\langle i,j \rangle \in \boldsymbol{R}} \hat{S}_i \cdot \hat{S}_j \tag{B1}$$

Here J parametrizes the strength of the spin-$\frac{1}{2}$'s if the two spins i, j belong to the *intersite* plaquette and λ parametrizes the strength of the spin-$\frac{1}{2}$'s if the two spins i, j belong to the *intrasite* plaquette. Obviously S_z is conserved and hence we have $U(1)$ symmetry.

If $\lambda = 0$ or $J = 0$, the model is exactly solvable and the ground state can be explicitly written out.[31] At these limits, the ground state is the simple product of the wavefunctions per each four spin-$\frac{1}{2}$'s connected by either by J or λ:

$$\begin{aligned} |P\rangle = &\frac{1}{2\sqrt{2}} \Big[|\uparrow\uparrow\downarrow\downarrow\rangle + |\downarrow\uparrow\uparrow\downarrow\rangle + |\uparrow\downarrow\downarrow\uparrow\rangle \Big] \\ &- \frac{1}{2} \Big[|\uparrow\downarrow\uparrow\downarrow\rangle + |\downarrow\uparrow\downarrow\uparrow\rangle \Big]. \end{aligned} \tag{B2}$$

The many-body order parameter can be constructed as following:

$$\hat{U}_2 = \exp\Big[\frac{2\pi i}{L_x L_y} \sum_{\boldsymbol{r}} xy (\hat{S}^z_{\boldsymbol{r}} - \bar{S}) \Big], \tag{B3}$$

where $\bar{S} = 2$ is introduced. This $\bar{S}$ is the average background spin density, which we subtract out. Using the exact ground states, we obtain that the topological state has $(-1) = \langle \hat{U}_2 \rangle$ (for $J \neq 0$ and $\lambda = 0$) and $(+1) = \langle \hat{U}_2 \rangle$ (for $J = 0$ and $\lambda \neq 0$).

Appendix C: Details on Tight-Binding Models

In this section, we summarize the physical properties and the symmetries of the tight-binding models for the topological insulator appearing in the main text.

1. Su-Schrieffer-Hegger chain

A minimal model for one-dimensional crystalline topological insulator is the Su-Schrieffer-Hegger (SSH) chain[26] which is a tight-binding model having alternating "weak" and "strong" hopping terms:

$$H_{\mathrm{SSH}} = \sum_r \Big[\big(\gamma c^\dagger_{r,1} c_{r,2} + \lambda c^\dagger_{r,2} c_{r+1,1} + \mathrm{h.c.}\big) + \delta\big(c^\dagger_{r,1} c_{r,1} - c^\dagger_{r,2} c_{r,2}\big)\Big], \tag{C1}$$

where $c^\dagger_{r,\alpha=1,2}$ is the electron creation operator at site r orbital α, γ and λ are inter- and intra-site hopping strengths, and δ is the onsite potential strength. Under the periodic boundary condition, it is convenient to work with the Bloch basis:

$$c^\dagger_{k,\alpha} = \frac{1}{\sqrt{L}} \sum_{r=1}^{L} e^{-ikr} c^\dagger_{r,\alpha}, \tag{C2}$$

where $k = \frac{2\pi n}{L}$ for some $n \in \mathbb{Z}$, $\alpha = 1, 2$ is the orbital index, and L is the system size. $c_{k,\alpha}$ can be defined analogously. The block Hamiltonian in terms of the Bloch state is given by

$$h_{\mathrm{SSH}}(k) = \begin{pmatrix} \delta & \gamma + \lambda e^{ik} \\ \gamma + \lambda e^{-ik} & -\delta \end{pmatrix}. \tag{C3}$$

2. Topological Quadrupole insulator

A minimal model for topological quadrupole insulator,[12] is given by

$$\begin{aligned} H = \sum_{\mathbf{r}} \Big[& \gamma_x \big(c^\dagger_{\mathbf{r},1} c_{\mathbf{r},3} + c^\dagger_{\mathbf{r},2} c_{\mathbf{r},4} + \mathrm{h.c.}\big) \\ & + \gamma_y \big(c^\dagger_{\mathbf{r},1} c_{\mathbf{r},4} - c^\dagger_{\mathbf{r},2} c_{\mathbf{r},3} + \mathrm{h.c.}\big) \\ & + \lambda_x \big(c^\dagger_{\mathbf{r},1} c_{\mathbf{r}+\hat{x},3} + c^\dagger_{\mathbf{r},4} c_{\mathbf{r}+\hat{x},2} + \mathrm{h.c.}\big) \\ & + \lambda_y \big(c^\dagger_{\mathbf{r},1} c_{\mathbf{r}+\hat{y},4} - c^\dagger_{\mathbf{r},3} c_{\mathbf{r}+\hat{y},2} + \mathrm{h.c.}\big) \\ & + \delta\big(c^\dagger_{\mathbf{r},1} c_{\mathbf{r},1} + c^\dagger_{\mathbf{r},2} c_{\mathbf{r},2} - c^\dagger_{\mathbf{r},3} c_{\mathbf{r},3} - c^\dagger_{\mathbf{r},4} c_{\mathbf{r},4}\big)\Big], \end{aligned} \tag{C4}$$

where $c^\dagger_{\mathbf{r},\alpha}$ and $c_{\mathbf{r},\alpha}$ are the fermion creation and annihilation operator at site $\mathbf{r} = (x, y)$ and $\alpha = 1, 2, 3, 4$ is the orbital index. If we impose the periodic boundary condition along x- and y-direction then it is convenient to work with the Bloch (momentum) basis

$$c^\dagger_{\mathbf{k},\alpha} = \frac{1}{\sqrt{L_x L_y}} \sum_{x=1}^{L_x} \sum_{y=1}^{L_y} e^{-i\mathbf{k}\cdot\mathbf{r}} c^\dagger_{\mathbf{r},\alpha},$$

where $\mathbf{k} = (k_x, k_y) = (\frac{2\pi n_x}{L_x}, \frac{2\pi n_y}{L_y})$ for some $n_x, n_y \in \mathbb{Z}$ is the Bloch momentum, $\alpha = 1, 2, 3, 4$ is the orbital index, and L_x and L_y is the system size along x- and y-direction. $c_{\mathbf{k},\alpha}$ is defined analogously. Using the Bloch basis, the Hamiltonian Eq. (C4) takes the block diagonal form

$$\begin{aligned} h(\mathbf{k}) = & \big(\gamma_x + \lambda_x \cos(k_x)\big)\Gamma_4 + \lambda_x \sin(k_x)\Gamma_3 \\ & + \big(\gamma_y + \lambda_y \cos(k_y)\big)\Gamma_2 + \lambda_y \sin(k_y)\Gamma_1 + \delta\Gamma_0, \end{aligned} \tag{C5}$$

where $\Gamma_0 = \tau_3 \otimes \tau_0$, $\Gamma_i = -\tau_2 \otimes \tau_i$ for $i = 1, 2, 3$, $\Gamma_4 = \tau_1 \otimes \tau_0$, where τ_0 is the 2×2 identity matrix and τ_i is the ith Pauli matrix. When $\delta = 0$, the physical energy band spectrum is gapless only when $|\gamma_x/\lambda_x| = 1$ and $|\gamma_y/\lambda_y| = 1$ while the Wannier gap closes when $|\gamma_x/\lambda_x| = 1$ or $|\gamma_y/\lambda_y| = 1$. The ground state at half-filling becomes a topological quadrupole insulator when $\delta = 0$, $|\gamma_x/\lambda_x| < 1$, and $|\gamma_y/\lambda_y| < 1$.

a. *Symmetries of the tight-binding model*

When $\delta = 0$ in Eq. (C4), there exists various symmetries which quantize the quadrupole moment $q_{xy} = 0, 1/2 \mod 1$. In the following, we summarize the symmetries of Eq. (C4) in the case of $\delta = 0$.

b. *Mirror symmetries*

With respect to the Bloch basis, x- and y-mirror symmetry can be written as

$$\hat{M}_x = i\tau_1 \otimes \tau_3 \quad \text{and} \quad \hat{M}_y = i\tau_1 \otimes \tau_1, \tag{C6}$$

and the block Hamiltonian Eq. (C5) transforms as

$$\begin{aligned} \hat{M}_x h(k_x, k_y) \hat{M}_x^{-1} &= h(-k_x, k_y) \quad \text{and} \\ \hat{M}_y h(k_x, k_y) \hat{M}_y^{-1} &= h(k_x, -k_y). \end{aligned} \tag{C7}$$

Because of the π flux threaded in each plaquette, two mirror symmetries do not commute but anticommute: $\{\hat{M}_x, \hat{M}_y\} = 0$.

c. *$\hat{C}_4$ symmetry*

When $\lambda_x = \lambda_y$ and $\gamma_x = \gamma_y$ in addition to $\delta = 0$, there exists $\hat{C}_4$ symmetry which also quantizes q_{xy}. With respect to the Bloch basis, the $\hat{C}_4$ symmetry can be represented as

$$\hat{r}_4 = \begin{pmatrix} 0 & \tau_0 \\ -i\tau_2 & 0 \end{pmatrix} \tag{C8}$$

and also

$$\hat{r}_4 h(k_x, k_y) \hat{r}_4^{-1} = h(k_y, -k_x) \tag{C9}$$

holds.

d. $\hat{C}_2$ symmetry

Even when $\delta \neq 0$, there exists $\hat{C}_2$ symmetry which quantizes the polarization in x- and y-direction. So when $|\delta|$ is small compared to other parameters in Eq. (C5), both x and y polarization are 0 hence the quadrupole moment q_{xy} is well-defined although it is no-longer quantized. With respect to the Bloch basis, the $\hat{C}_2$ operator can be represented as

$$\hat{r}_2 = -i\tau_0 \otimes \tau_2, \tag{C10}$$

and also

$$\hat{r}_2 h(\mathbf{k}) \hat{r}_2^{-1} = h(-\mathbf{k}) \tag{C11}$$

holds.

e. Symmetry breaking perturbations

Here, we present how onsite symmetry breaking perturbations affect the bulk quadrupole moment defined as a complex phase of $\langle \hat{U}_2 \rangle$ when perturbing away from a topological quadrupole insulator point. In adding perturbations, we still want to keep $\hat{C}_2$ symmetry as this would enforce the quantization of polarization in x- and y-direction, i.e., total polarization remains zero when the perturbation is small.

Starting from the $\hat{C}_2$ operator Eq. (C10), one can classify 4×4 matrices that commute with $\hat{r}_2$. The general form of such matrix can be expressed as

$$H_{\text{pert}} = \begin{pmatrix} a_r\tau_0 + c_r\tau_2 & e_c\tau_0 + f_c\tau_2 \\ e_c^*\tau_0 + f_c^*\tau_2 & b_r\tau_0 + d_r\tau_2 \end{pmatrix}, \tag{C12}$$

where a_r, b_r, c_r, d_r are real parameters, e_c and f_c are complex parameters, and asterisk denotes the complex conjugation. One can immediately see that δ term in Eq. (C5) is reproduced when $a_r = -b_r = \delta$ and set all the other coefficients to zero in Eq. (C12). Let us also note that when ($a_r = b_r = 0$, $c_r = -d_r$, $e_c = -if_c \in \mathbb{R}$), Eq. (C12) preserves two mirror symmetries and when ($a_r = b_r = 0$, $c_r = d_r$, $e_c = -if_c \in \mathbb{R}$), Eq. (C12) preserves $\hat{C}_4$ symmetry.

One can check numerically that when the perturbation Eq. (C12) is *onsite*, only nonzero a_r and b_r do change the quadrupole moment whereas other terms does not. When a_r and b_r are nonzero, we can always add an identity matrix with some coefficient so that the perturbation reduces to the δ term in Eq. (C5). Hence Eq. (C5) is quite generic.

Appendix D: Miscellaneous Observations on Many-Body Order Parameters

Here we present several miscellaneous observations on many-body order parameters. This includes the scaling behavior of $|\langle \hat{U}_a \rangle|$ and the dependence on the coordinate re-parametrizations. To be concrete, we concentrate on the polarization $\hat{U}_1$ and quadrupolar moment $\hat{U}_2$.

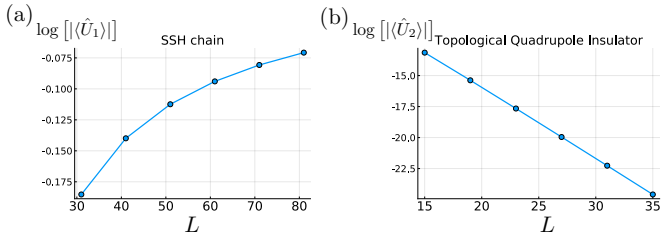

FIG. 9. Scaling of many-body order parameters $|\langle \hat{U}_{n=1,2} \rangle|$ versus the linear system size L in the case of (a) SSH chain Eq. (C3) with $(\gamma, \lambda, \delta) = (1.0, 2.0, 0.1)$ and (b) topological quadrupole insulator Eq. (C5) with $(\gamma_x, \gamma_y, \lambda_x, \lambda_y, \delta) = (1.0, 1.0, 2.0, 2.0, 0.1)$. (a) The modulus of $\langle \hat{U}_1 \rangle$ converges to 1 as $L \to \infty$, as expected in the case of a gapped insulator. (b) The modulus of $\langle \hat{U}_2 \rangle$ decays exponentially in L even in the case of a gapped insulator.

1. Scaling of $|\langle \hat{U}_a \rangle|$

a. Scaling of $|\langle \hat{U}_1 \rangle|$

Here we summarize the known scaling forms of the modulus of the expectation value of $\hat{U}_1$, which is introduced by Resta [5]. For an one-dimensional system with system size L, the Resta's operator is given by

$$\hat{U}_1 = \exp\left(\frac{2\pi i}{L} \sum_{x=1}^{L} x \hat{n}_x\right), \tag{D1}$$

where $\hat{n}_x = \sum_\alpha c_{x,\alpha}^\dagger c_{x,\alpha}$ is the occupation number operator at site x with α being the orbital index and we label the position at site x to $x = 1, 2, \cdots, L$. Eq. (D1) is well-defined in the sense that upon re-labeling a position x by $x + L$, $\hat{U}_1$ remains invariant. Moreover, in the case of a band insulator, the expectation value of $\hat{U}_1$ is related to the Zak phase by (up to an additional minus sign which we address in detail below)

$$\frac{1}{2\pi} \text{Im}\big(\log \langle \hat{U}_1 \rangle\big) = \int_{\text{BZ}} dk \ \text{tr}\big(\mathcal{A}_k\big) + \mathcal{O}\big(1/L\big) \mod 1, \tag{D2}$$

where the expectation value in the LHS is with respect to the many-body ground state, the integral in the RHS is the Zak phase[4] with BZ denotes the one dimensional Brillouin Zone, $\mathcal{A}_k$ is the Berry connection, and $\mathcal{O}(1/L)$ term vanishes as the system size $L \to \infty$. This provides a proof that the phase of the expectation value of $\hat{U}_1$ detects the polarization, as the polarization is equal to the Zak phase in a proper unit.

Although the complex phase of $\langle \hat{U}_1 \rangle$ gives the electric polarization, its modulus also captures invaluable information, e.g., the localization length of the ground state.[6]

In FIG. 9, we provide the scaling of (a) $|\langle\hat{U}_1\rangle|$ for the SSH chain Eq. (C3) with $(\gamma, \lambda, \delta) = (1.0, 2.0, 0.1)$ versus the linear system size L. In this case, the bulk gap is finite. As expected, when the linear system size $L \to \infty$, $|\langle\hat{U}_1\rangle| \to 1$ in the case of the SSH chain. In general, when the bulk gap is nonzero, the modulus of the expectation value $|\langle U_1\rangle|$ converges to a positive number as $L \to \infty$. On the other hand, at critical point $|\langle U_1\rangle|$ vanishes as $L \to \infty$ and it is conjectured to obey the following scaling relation:[37]

$$|\langle\hat{U}_1\rangle| \sim \frac{1}{L^\beta}, \tag{D3}$$

where $\beta > 0$ is the exponent characterizing the decay in the thermodynamic limit.

b. *Scaling of* $|\langle\hat{U}_2\rangle|$

Here we perform the scaling study of $|\langle\hat{U}_2\rangle|$ with respect to the length and the Wannier gap. Recall that $\hat{U}_2$ is

$$\hat{U}_2 = \exp\left(\frac{2\pi i}{L_x L_y}\sum_{x=1}^{L_x}\sum_{y=1}^{L_y} xy\hat{n}_{(x,y)}\right), \tag{D4}$$

where $\hat{n}_{(x,y)}$ is the occupation number operator at site (x, y) and we label the x- (y-)position of site (x, y) as $x = 1, 2, \cdots, L_x$ ($y = 1, 2, \cdots, L_y$).

First of all, at least within the finite-size calculation up to $L \sim 20$ and within the toy model, we found that, unlike $|\langle\hat{U}_1\rangle|$, $|\langle\hat{U}_2\rangle|$ seems to exhibit the exponential decay in $L = L_x = L_y$ as shown in FIG. 9 (b), even for the insulating ground state (here the Wannier bands are also gapped).

$$|\langle\hat{U}_2\rangle| \sim e^{-\alpha L}, \tag{D5}$$

where $\alpha > 0$ is an exponent characterizing the exponential decay. *However, to conclude that this scaling behavior is generic for any insulator, we need more detailed and thorough calculations on various models. Keeping this in mind, at this moment we would like to modestly mention that the scaling behaviors of the modulus of* $\langle\hat{U}_2\rangle$ *is quite different from those of* $\hat{U}_1$. Despite of exponentially vanishing modulus for the models that we consider, the complex phases of the expectation value can be reliably measured for the typical system sizes that we worked on, e.g., $L \sim 10 - 20$. We also have checked that the Dirac semimetal state, which has a zero energy gap, also shows an exponential decay (with different exponent) in system size L.

Second, we perform the comparative studies of the modulus with the Wannier gap. For this we use the model of the topological quadrupole insulator Eq. (C5) with $\delta = 0$. Here the topological-to-trivial quadrupole insulator transition is associated with the Wannier gap closing

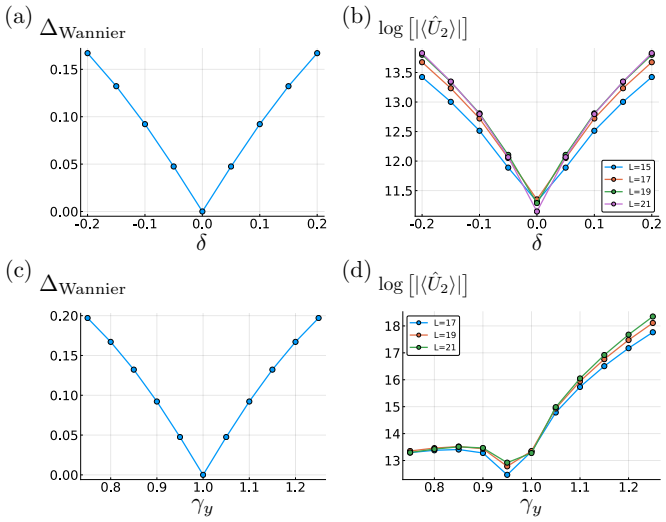

FIG. 10. Comparison between the Wannier gap and the modulus of $|\langle\hat{U}_2\rangle|$ for topological quadrupole insulator Eq. (C4). In (a) and (b) we fix $(\gamma_x, \gamma_y, \lambda_y, \lambda_x, \lambda_y) = (0.75, 1.0, 1.0, 1.0)$ and tune $\delta \in [-0.2, 0.2]$. When $\delta = 0$ (a) the Wannier gap closes and (b) $|\langle\hat{U}_2\rangle|$ is the smallest. In (c) and (d) we fix $(\gamma_x, \lambda_x, \lambda_y, \delta) = (0.75, 1.0, 1.0, 0.0)$ and tune $\gamma_y \in [0.75, 1.25]$. (c) The Wannier gap associated with the Wannier band $\nu_x(k_y)$ closes at $\gamma_y = 1.0$ and (d) $|\langle\hat{U}_2\rangle|$ is the smallest around $\gamma_y = 1.0$. In all cases, the Wannier gap is well-defined in the thermodynamic limit while $|\langle\hat{U}_2\rangle|$ vanishes in the thermodynamic limit.

transition while the bulk gap may not close at the transition point.[12] To see how $\langle\hat{U}_2\rangle$ detects such quantum phase transition, we compute $|\langle\hat{U}_2\rangle|$ across the phase transition. Due to the quantization by symmetries, $\langle\hat{U}_2\rangle$ is a real number and changes its sign across the phase transition. So precisely at the transition point, $\langle\hat{U}_2\rangle$ vanishes up to the correction from finite-size effect. In FIG. 10, we present two scenarios of Wannier-gap closing transition, one by tuning δ and the other by tuning λ_y. In FIG. 10 (a) and (b), we fix $(\gamma_x, \gamma_y, \lambda_x, \lambda_y) = (0.75, 1.0, 1.0, 1.0)$ and tune $\delta \in [-0.2, 0.2]$. When $\delta = 0$, Wannier gap closes and $|\langle\hat{U}_2\rangle|$ becomes the smallest. In FIG. 10 (c) and (d), we fix $(\gamma_x, \lambda_x, \lambda_y, \delta) = (0.75, 1.0, 1.0, 0.0)$ and tune $\gamma_y \in [0.75, 1.25]$. When $\gamma_y < 1$, the half-filled ground state is the topological quadrupole insulator and when $\gamma_y > 1$, the half-filled ground state is trivial. In FIG. 10 (c), we compute the Wannier gap associated with the Wannier bands $\nu_x(k_y)$. We see that the minimum of $|\langle\hat{U}_2\rangle|$ occurs around the phase transition point $\gamma_y = 1.0$.

2. Generalized Many-Body Operators

a. *Many-Body Opertors acting on Subsystem*

In the main text, we generalize our many-body operators Eq. (19) and Eq. (20) which act only on the sub-

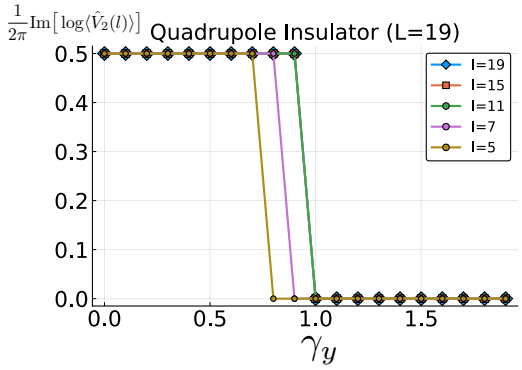

FIG. 11. Many-body order parameter based on $\hat{V}_2(l)$ applied to Eq. (C4) for various l's with $(\gamma_x, \lambda_x = \lambda_y, \delta) = (0.5, 1.0, 0.0)$ while changing γ_y, which is the same as the cut used in FIG. 4 (c). The curve is identical for $l = 19, 15$, and 11, showing that even when l is an order of $L/2$, the many-body order parameter based on $\hat{V}_2(l)$ correctly reproduce the phase diagram along the cut.

system, based on the reasoning from the effective field theory. Here, we examine the validity of such operators by focusing on quadrupole case with quantizing symmetries remains intact. Specifically, in FIG. 11, we test whether the operator $\hat{V}_2(l)$ Eq. (20) can reproduce the phase diagram presented in FIG. 4 (a). As can be seen in the figure, up to l being an order of the half of the full system size, the many-body order parameter based on $\hat{V}_2(l)$ correctly reproduce the phase diagram. Furthermore, even when $l = 5$, which is an order of 1/4 of the full system size, the many-body operator fails only near the phase transition (Wannier gap closing point, which is at $\gamma_y = 1.0$), and works perfectly well in the other regimes.

b. *Dependence on Coordinate Parameterization*

As outlined in the main text, our many-body operators as well as the original Resta's operator can be generalized by acting only on subsystem and/or change in the boundary conditions. In this subsection, we would like to discuss the dependence on the coordinate parametrization on the many-body operators. To be precise, let us consider the following many-body operator which fully takes into account both the partial action and the coordinate parametrization issue.

$$\hat{V}_1(l,d) = \begin{cases} \exp\left[\frac{2\pi i}{l}\sum_x (x-d)(\hat{n}_x - \overline{n})\right] & \text{for } x \in [1,l] \\ 1 & \text{otherwise,} \end{cases} \tag{D6}$$

where we consider a finite system with size L, $l > 0$ is an integer smaller than or equal to L, atomic sites are labeled by $x \in \{1, 2, \cdots, L\}$, and $\overline{n}$ is the average filling per site. Similarly for quadrupole moment,

$$\hat{V}_2(l,d) = \begin{cases} \exp\left[\frac{2\pi i}{l^2}\sum_{\mathbf{r}=(x,y)} (x-d)(y-d)(\hat{n}_{\mathbf{r}} - \overline{n})\right] & \text{for } \mathbf{r} \in [1,l]\times[1,l] \\ 1 & \text{otherwise} \end{cases}, \tag{D7}$$

where the whole system size is given by (L, L), $l > 0$ is an integer less than or equal to L, sites are labeled by $x, y \in \{1, 2, \cdots, L\}$, and $\overline{n}$ denotes the average filling per site. Here, we present the isotropic case, but anisotropic as well as generalization to higher-order moments is immediate. Note that these are almost the same as the formula Eq. (19) and Eq. (20) in the main text, but with an extra phase factors $\propto \exp(2\pi i \overline{n})$, which is the contribution from background positive charges. Here d parametrizes the dependence on the "origin" of the coordinate systems.

Now we present numerical evaluation of $\hat{V}_1(l,d)$ Eq. (D6) and $\hat{V}_2(l,d)$ Eq. (D7) in the case of SSH chain Eq. (C3) and topological quadrupole insulator Eq. (C5). Here, l denotes the linear system size within which the operator $V_n(l,d)$ acts nontrivially and d tunes the choice of the origin of our system. In FIG. 12, we present the results for $\delta = 0$ and $\delta = 0.1$, where the former has the quantization symmetries and the latter does not. We set $(\gamma, \lambda) = (1.0, 2.0)$ for FIG. 12 (a) and (c), and set $(\gamma_x, \gamma_y, \lambda_x, \lambda_y) = (1.0, 1.0, 2.0, 2.0)$ for FIG. 12 (b) and (d). Hence for FIG. 12 (a) (FIG. 12 (b)), the ground state has topologically nontrivial polarization (quadrupole moment).

As expected, when $l = L$, $\langle\hat{V}_1(l = L, d)\rangle$, which is the original Resta's operator, is independent of d due to the charge conservation in the ground state. However, this is no longer true for $\langle\hat{V}_1(l < L, d)\rangle$ and $\langle\hat{V}_2(l,d)\rangle$ for all l, which is summarized in FIG. 12 (a) and (b). As a result, for some choices of l and d, the complex phase of $\langle\hat{V}_n(l,d)\rangle$ fails in capturing the ground state topological multipole moments. When $\delta = 0.1$, quantization of $\langle\hat{V}_n(l,d)\rangle$ no longer exists and its complex phase can take arbitrary value, which can be seen in FIG. 12 (c) and (d).

This behavior can be easily explained by considering the ultra-short correlated states. For the illustrational purpose, we take the topological and trivial ground states

of the polarization chain.

$$|GS_{\rm triv}\rangle = \prod_{n\in\mathbb{Z}} |n\rangle, \quad |GS_{\rm top}\rangle = \prod_{n\in\mathbb{Z}} |n+\frac{1}{2}\rangle. \tag{D8}$$

For these ground states, we see that $\langle GS_{\rm triv}|\hat{V}_1(l,\frac{l}{2})|GS_{\rm triv}\rangle = \langle GS_{\rm top}|\hat{V}_1(l,\frac{l}{2})|GS_{\rm top}\rangle = 1$, signaling that the two states cannot be distinguished if $d = \frac{l}{2}$. Similar discussion can be made for the quadrupolar insulators, too, and this explains the lumps appearing in the numerical data Fig. 12.

One may worry about "this coordinate choice dependence on the value of $\langle\hat{U}_2\rangle$"[35] since the original Resta's formula does not have such behaviors. Though such invariance is certainly desirable, we would like to remark that, in principle, the independence of the coordinate choice is not a requirement for the order parameters of the multipoles. For instance, as far as the coordinate system is chosen as we prescribed, i.e., $(x,y) \in (0,L_x]\times(0,L_y]$, our formula works for several non-trivial cases as described in our main text and for e.g., amorphous systems[33] and sonic systems.[34] In practice, any coordinate choice except a few very particular coordinate choice (as discussed in this supplemental section) works equally well as the choice $(x,y) \in (0,L_x]\times(0,L_y]$ we used in the main text.

Appendix E: Application of Many-Body Order Parameter $\hat{U}_2$ on Generic C_4-Symmetric Insulators

Recently, a new class of insulators in two dimensions, called C_n-symmetric insulators, are introduced[20] in which a fractional charges can be localized in a corner when the system is subject to full open boundary condition, similar to quadrupole insulators. C_n-symmetric insulators can be understood in terms of "filling anomaly" which counts the number of excessive or deficit of electrons between electrons at constant filling and electrons satisfying the charge neutrality.[20] As a result of a nonzero filling anomaly, fractional charges are localized in all corners in a C_n respecting manner *only when* the bulk polarization becomes zero. To better understand our many-body operator $\hat{U}_2$ and its relation to nested Wilson loop, let us focus on C_4-symmetric cases with zero polarizations in Ref. 20. We consider two models – 1) $h^{(4)}_{1b} + h^{(4)}_{2c}$, a model with average filling 3/8 and corner charge 1/4, and 2) $h^{(4)}_{2b}$, a model with 1/2 filling and corner charge 1/2, – where we use the notation introduced in Ref. 20. For these states, because they do not posses the gap in the Wannier bands and so do not have the quadrupole order (the nested Wilson loop indices require non-vanishing Wannier gaps), we expect the many-body order parameter, i.e., the phase value Q_{xy} of $\hat{U}_2$, to exhibit unstable continuum values instead of quantized values matching the corner charge. We explicitly confirm these from the calculations below.

1. $h^{(4)}_{1b} + h^{(4)}_{2c}$ model

$h^{(4)}_{1b}$ is a four-band model which has "corner charge" $e/4$ at 1/4 filling. $h^{(4)}_{2c}$ is also a four-band model which has 0 "corer charge" at 1/2 filling. Since both $h^{(4)}_{1b}$ and $h^{(4)}_{2c}$ have polarization $\mathbf{P} = (\frac{e}{2},\frac{e}{2})$, we stack them together so that the net polarization becomes 0.[20] Following Ref. 20, we turn on onsite hopping terms between orbitals of $h^{(4)}_{1b}$ and $h^{(4)}_{2c}$. The Bloch Hamiltonian is given by,

$$h^{(4)}_{1/4}(\mathbf{k}) = \begin{pmatrix} h^{(4)}_{1b}(\mathbf{k}) & \gamma_c \\ \gamma_c^\dagger & h^{(4)}_{2c}(\mathbf{k}), \end{pmatrix} \tag{E1}$$

where

$$h^{(4)}_{1b}(\mathbf{k}) = \begin{pmatrix} 0 & t+e^{ik_x} & 0 & t+e^{ik_y} \\ t+e^{-ik_x} & 0 & t+e^{ik_y} & 0 \\ 0 & t+e^{-ik_y} & 0 & t+e^{-ik_x} \\ t+e^{-ik_y} & 0 & t+e^{ik_x} & 0 \end{pmatrix}, \tag{E2}$$

$$h^{(4)}_{2c}(\mathbf{k}) = \begin{pmatrix} 0 & 0 & t+1.5e^{ik_x} & 0 \\ 0 & 0 & 0 & t+1.5e^{ik_y} \\ t+1.5e^{-ik_x} & 0 & 0 & 0 \\ 0 & t+1.5e^{-ik_y} & 0 & 0 \end{pmatrix}, \tag{E3}$$

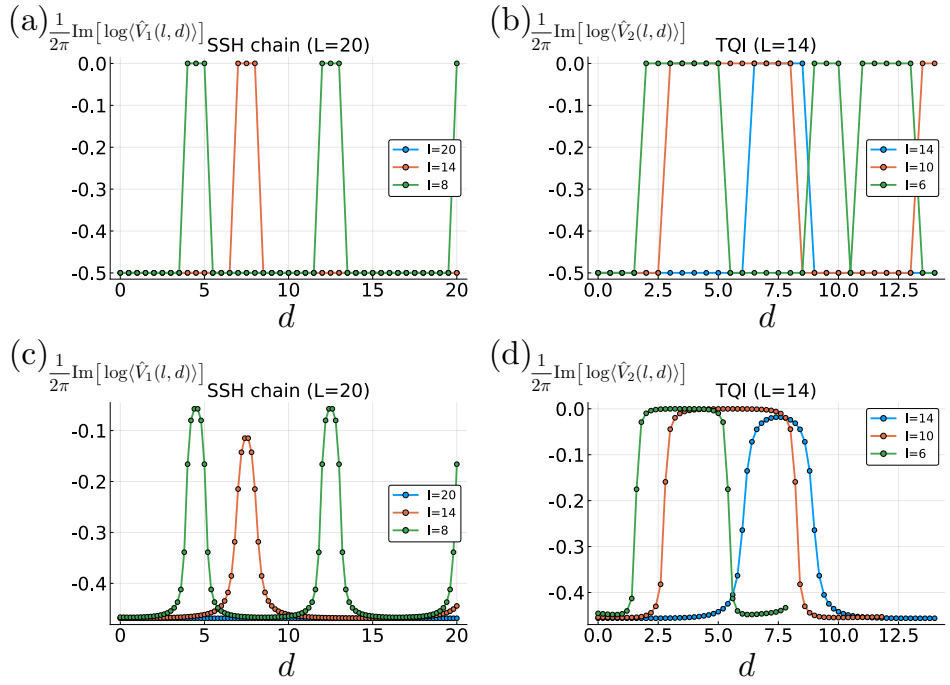

FIG. 12. The complex phase of $\langle\hat{V}_1(l,d)\rangle$ and $\langle\hat{V}_2(l,d)\rangle$ for various l's as a function of d. (a) and (c) correspond to the SSH chain Eq. (C3) where we set $(\gamma,\lambda)=(1.0,2.0)$ and (c) $\delta=0$ and (d) $\delta=0.1$. (b) and (d) correspond to the topological quadrupole insulator Eq. (C5) where we set $(\gamma_x,\gamma_y,\lambda_x,\lambda_y)=(1.0,1.0,2.0,2.0)$ and (c) $\delta=0$ and (d) $\delta=0.1$. While the ground state of (a) and (b) are topologically nontrivial, for some l and d, the complex phase of $\langle\hat{V}_n(l,d)\rangle$ becomes trivial. In (c) and (d), as a function of d, we see "lumps".

and

$$\gamma_c=\begin{pmatrix} t & t & 0 & 0\\ 0 & t & t & 0\\ 0 & 0 & t & t\\ t & 0 & 0 & t\end{pmatrix}. \tag{E4}$$

Under the full open boundary condition, Eq. (E1) at 3/8 filling have quantized corner charge $3|e|/4$ localized at each corner.[20] While the corner charge remains quantized and localized when tuning the hopping parameter t from 0 to 0.25, the expectation value of $\hat{U}_2$ is not, as shown in FIG. 13 (a) where strong even-odd effect is also shown. The Wannier band is shown in FIG. 13 (b), where two degenerate and one non-degenerate flat bands are shown. This indicates that Eq. (E1) at 3/8 filling does not have a stable quadrupole moment in the bulk, which is well reflected in our many-body operator $\hat{U}_2$. Note also that the Wannier gap closes, so that the nested Wilson loop indices are not well defined,[12] which is consistent with the unstable behavior of $\hat{U}_2$ with respect to the ground state of Eq. (E1) at 3/8 filling.

2. $h^{(4)}_{2b}$ model

$h^{(4)}_{2b}$ is a four-band model which has corner charge $e/2$ and vanishing polarization $\mathbf{P}=0$ at 1/2 filling. The Bloch Hamiltonian is given by

$$h^{(4)}_{1/2}(\mathbf{k})\equiv h^{(4)}_{2b}(\mathbf{k})=\begin{pmatrix} \delta & t & e^{i(k_x+k_y)} & t\\ t & -\delta & t & e^{i(k_y-k_x)}\\ e^{-i(k_x+k_y)} & t & \delta & t\\ t & e^{i(k_x-k_y)} & t & -\delta\end{pmatrix}, \tag{E5}$$

where t is the intra-site hopping parameter and δ is the strength of an onsite C_4-symmetry breaking term. When $0<t<1$ and $\delta=0$, the ground state at half-filling is a C_4-symmetric insulator having zero polarization as well as

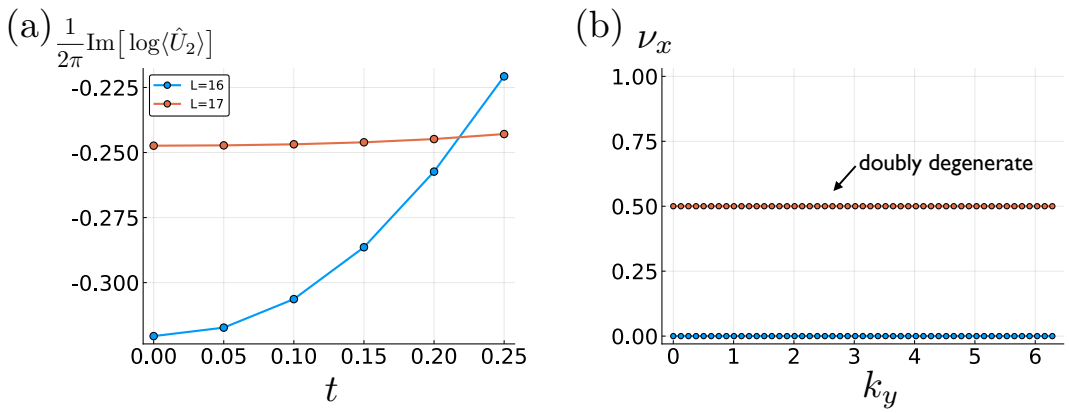

FIG. 13. (a) $\frac{1}{2\pi}\mathrm{Im}\log\langle\hat{U}_2\rangle$ as a function of hopping parameter t in Eq. (E1) with system sizes $L = 16$ and $L = 17$. For $L = 16$, we take into account additional (-1) factor coming from background charge distribution. Note that both $L = 16$ and $L = 17$ show dependency in t while the fractional corner charge is independent of $t \in [0, 0.25]$, hence indicating an unstable nature of C_4-insulator with respect to $\hat{U}_2$. (b) The Wannier band $\nu_x(k_y)$ of the ground state of Eq. (E1) at 3/8 filling. We have one doubly degenerate and one non-degenerate flat bands so that in total zero net polarization.

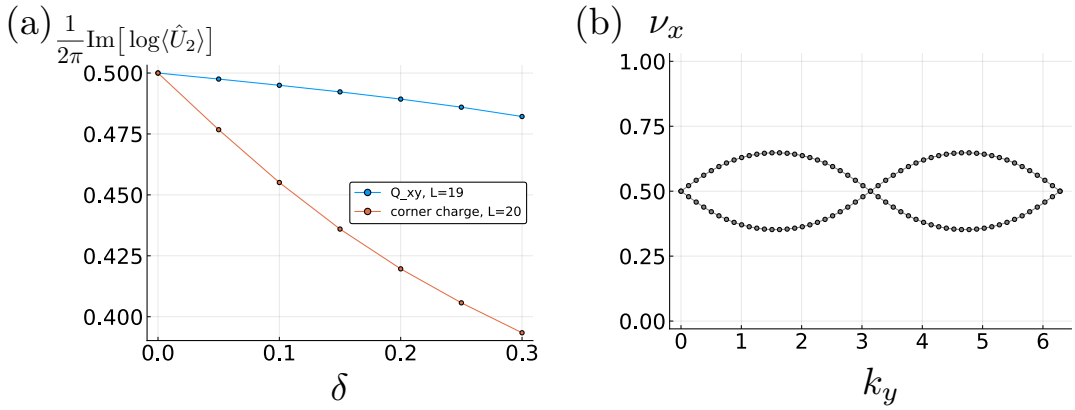

FIG. 14. (a) $\frac{1}{2\pi}\mathrm{Im}\log\langle\hat{U}_2\rangle$ as a function of onsite C_4-breaking parameter δ in Eq. (E5) with $t = 0.3$. Because of finite δ, corner charge changes smoothly from a quantized value 0.5. Note that there is a mismatch between the corner charge and $\frac{1}{2\pi}\mathrm{Im}\log\langle\hat{U}_2\rangle$, showing an unstable nature of C_4-symmetric insulator with respect to $\hat{U}_2$. (b) The Wannier band $\nu_x(k_y)$ of the ground state of Eq. (E5) with $t = 0.3$ and $\delta = 0.3$ and at 1/2 filling. The Wannier band becomes gapless at $k_y = 0, \pi$.

1/2 corner charge localized at each corner. Moreover, $\frac{1}{2\pi}\mathrm{Im}\log\langle\hat{U}_2\rangle$ equals 0.5 (0) when L is odd (even), as in the case of topological quadrupole insulators. However, upon introducing symmetry breaking term, i.e., $\delta \neq 0$, there exists a mismatch between $\frac{1}{2\pi}\mathrm{Im}\log\langle\hat{U}_2\rangle$ and the corner charge as shown in FIG. 14 (a). The Wannier band is shown in FIG. 14 (b), where we see that the Wannier band is gapless at $k_y = 0$ and π. Since the Wannier bands are gapless the nested Wilson loop indices are not well defined,[12] This fact is consistent with the unstable behavior of $\hat{U}_2$ with respect to the ground state of Eq. (E5) at 1/2 filling.

* Electronic Address: gilyoungcho@postech.ac.kr

[1] Raffaele Resta, "Macroscopic polarization in crystalline dielectrics: the geometric phase approach," Rev. Mod. Phys. **66**, 899–915 (1994).
[2] M. Z. Hasan and C. L. Kane, "Colloquium: Topological insulators," Rev. Mod. Phys. **82**, 3045–3067 (2010).
[3] Xiao-Liang Qi and Shou-Cheng Zhang, "Topological insulators and superconductors," Rev. Mod. Phys. **83**, 1057–1110 (2011).
[4] J. Zak, "Berry's phase for energy bands in solids," Phys. Rev. Lett. **62**, 2747–2750 (1989).
[5] Raffaele Resta, "Quantum-mechanical position operator in

extended systems," Phys. Rev. Lett. **80**, 1800–1803 (1998).
[6] Raffaele Resta and Sandro Sorella, "Electron localization in the insulating state," Phys. Rev. Lett. **82**, 370–373 (1999).
[7] R. Nourafkan and G. Kotliar, "Electric polarization in correlated insulators," Phys. Rev. B **88**, 155121 (2013).
[8] Masaaki Nakamura and Synge Todo, "Order parameter to characterize valence-bond-solid states in quantum spin chains," Phys. Rev. Lett. **89**, 077204 (2002).
[9] Gil Young Cho, Chang-Tse Hsieh, Takahiro Morimoto, and Shinsei Ryu, "Topological phases protected by reflection symmetry and cross-cap states," Phys. Rev. B **91**, 195142 (2015).
[10] Hassan Shapourian, Ken Shiozaki, and Shinsei Ryu, "Many-body topological invariants for fermionic symmetry-protected topological phases," Phys. Rev. Lett. **118**, 216402 (2017).
[11] Wladimir A. Benalcazar, B. Andrei Bernevig, and Taylor L. Hughes, "Quantized electric multipole insulators," Science **357**, 61–66 (2017).
[12] Wladimir A. Benalcazar, B. Andrei Bernevig, and Taylor L. Hughes, "Electric multipole moments, topological multipole moment pumping, and chiral hinge states in crystalline insulators," Phys. Rev. B **96**, 245115 (2017).
[13] Josias Langbehn, Yang Peng, Luka Trifunovic, Felix von Oppen, and Piet W. Brouwer, "Reflection-symmetric second-order topological insulators and superconductors," Phys. Rev. Lett. **119**, 246401 (2017).
[14] Zhida Song, Zhong Fang, and Chen Fang, "$(d-2)$-dimensional edge states of rotation symmetry protected topological states," Phys. Rev. Lett. **119**, 246402 (2017).
[15] Frank Schindler, Ashley M. Cook, Maia G. Vergniory, Zhijun Wang, Stuart S. P. Parkin, B. Andrei Bernevig, and Titus Neupert, "Higher-order topological insulators," Science Advances **4** (2018), 10.1126/sciadv.aat0346.
[16] Frank Schindler, Zhijun Wang, Maia G Vergniory, Ashley M Cook, Anil Murani, Shamashis Sengupta, Alik Yu Kasumov, Richard Deblock, Sangjun Jeon, Ilya Drozdov, Hlne Bouchiat, Sophie Guron, Ali Yazdani, B. Andrei Bernevig, and Titus Neupert, "Higher-order topology in bismuth," Nature Physics **14**, 918 (2018).
[17] Motohiko Ezawa, "Minimal models for wannier-type higher-order topological insulators and phosphorene," Phys. Rev. B **98**, 045125 (2018).
[18] Luka Trifunovic and Piet Brouwer, "Higher-order bulk-boundary correspondence for topological crystalline phases," arXiv preprint arXiv:1805.02598 (2018).
[19] S. Franca, J. van den Brink, and I. C. Fulga, "An anomalous higher-order topological insulator," Phys. Rev. B **98**, 201114 (2018).
[20] Wladimir A. Benalcazar, Tianhe Li, and Taylor L. Hughes, "Quantization of fractional corner charge in c_n-symmetric topological crystalline insulators," arXiv preprint arXiv:1809.02142 (2018).
[21] For the systems with even $L_x \cdot L_y$, there is an additional minus sign (which can also be noticed in Resta's original paper[5]) but the similar discussion can be straightforwardly made by noting that the topological part of the quadrupole moments are defined as the relative deviation from that of the trivial insulators. In the remaining text, we always take into account this (possible) additional sign factor when evaluating $\hat{U}_a$. Note that the sign factor can also be computed by evaluating $\hat{U}_a$ for background positive charge distribution.
[22] Haruki Watanabe and Masaki Oshikawa, "Inequivalent berry phases for the bulk polarization," Phys. Rev. X **8**, 021065 (2018).
[23] Jeffrey Goldstone and Frank Wilczek, "Fractional quantum numbers on solitons," Phys. Rev. Lett. **47**, 986–989 (1981).
[24] Xiao-Liang Qi, Taylor L. Hughes, and Shou-Cheng Zhang, "Topological field theory of time-reversal invariant insulators," Phys. Rev. B **78**, 195424 (2008).
[25] Ian Affleck and Elliott H. Lieb, "A proof of part of haldane's conjecture on spin chains," Letters in Mathematical Physics **12**, 57–69 (1986).
[26] W. P. Su, J. R. Schrieffer, and A. J. Heeger, "Solitons in polyacetylene," Phys. Rev. Lett. **42**, 1698–1701 (1979).
[27] David Vanderbilt and R. D. King-Smith, "Electric polarization as a bulk quantity and its relation to surface charge," Phys. Rev. B **48**, 4442–4455 (1993).
[28] Jun-Won Rhim, Jan Behrends, and Jens H. Bardarson, "Bulk-boundary correspondence from the intercellular zak phase," Phys. Rev. B **95**, 035421 (2017).
[29] We thank the anonymous referee for bringing our attention to this example.
[30] Byungmin Kang and Gil Young Cho, in preparation.
[31] Oleg Dubinkin and Taylor L Hughes, "Higher order bosonic topological phases in spin models," arXiv preprint arXiv:1807.09781 (2018).
[32] Yizhi You, Trithep Devakul, F. J. Burnell, and Titus Neupert, "Higher-order symmetry-protected topological states for interacting bosons and fermions," Phys. Rev. B **98**, 235102 (2018).
[33] Adhip Agarwala, Vladimir Juricic, and Bitan Roy, "Higher order topological insulators in amorphous solids," arXiv preprint arXiv:1902.00507 (2019).
[34] Zhi-Kang Lin, Hai-Xiao Wang, Ming-Hui Lu, and Jian-Hua Jiang, "Nonsymmorphic topological quadrupole insulator in sonic crystals," arXiv preprint arXiv:1903.05997 (2019).
[35] Seishiro Ono, Luka Trifunovic, and Haruki Watanabe, "Difficulties in operator-based formulation of the bulk quadrupole moment," arXiv preprint arXiv:1902.07508 (2019).
[36] William A. Wheeler, Lucas K. Wagner, and Taylor L. Hughes, "Many-body electric multipole operators in extended systems," arXiv preprint arXiv:1812.06990 (2018).
[37] Ryohei Kobayashi, Yuya O. Nakagawa, Yoshiki Fukusumi, and Masaki Oshikawa, "Scaling of the polarization amplitude in quantum many-body systems in one dimension," Phys. Rev. B **97**, 165133 (2018).